


 Cite this: *RSC Adv.*, 2023, **13**, 12889

New pyrazolopyridine and pyrazolothiazole-based compounds as anti-proliferative agents targeting c-Met kinase inhibition: design, synthesis, biological evaluation, and computational studies†

 Zahra M. Alamshany,^a Eman M. Algamdi,^a Ismail M. M. Othman,^b Manal M. Anwar^{id, c*} and Eman S. Nossier^{*de}

c-Met tyrosine kinase plays a key role in the oncogenic process. Inhibition of the c-Met has emerged as an attractive target for human cancer treatment. This work deals with the design and synthesis of a new set of derivatives bearing pyrazolo[3,4-*b*]pyridine, pyrazolo[3,4-*b*]thieno[3,2-*e*]pyridine, and pyrazolo[3,4-*d*]thiazole-5-thione scaffolds, **5a,b**, **8a-f**, and **10a,b**, respectively, utilizing 3-methyl-1-tosyl-1*H*-pyrazol-5(4*H*)-one (**1**) as a key starting material. All the new compounds were evaluated as antiproliferative agents against HepG-2, MCF-7, and HCT-116 human cancer cell lines utilizing 5-fluorouracil and erlotinib as two standard drugs. Compounds **5a,b** and **10a,b** represented the most promising cytotoxic activity of IC_{50} values ranging from 3.42 ± 1.31 to $17.16 \pm 0.37 \mu\text{M}$. Both **5a** and **5b** showed the most cytotoxicity and selectivity toward HepG-2, with IC_{50} values of $3.42 \pm 1.31 \mu\text{M}$ and $3.56 \pm 1.5 \mu\text{M}$, respectively. The enzyme assay demonstrated that **5a** and **5b** had inhibition potency on c-Met with IC_{50} values in nanomolar range of 4.27 ± 0.31 and $7.95 \pm 0.17 \text{ nM}$, respectively in comparison with the reference drug cabozantinib (IC_{50} : $5.38 \pm 0.35 \text{ nM}$). The impact of **5a** on the cell cycle and apoptosis induction potential in HepG-2 and on the apoptotic parameters; Bax, Bcl-2, p53, and caspase-3 was also investigated. Finally, the molecular docking simulation of the most promising derivatives **5a** and **5b** was screened against c-Met to investigate the binding patterns of both compounds in the active site of the c-Met enzyme. *In silico* ADME studies were also performed for **5a** and **5b** to predict their physicochemical and pharmacokinetic characteristics.

 Received 24th March 2023
 Accepted 13th April 2023

 DOI: 10.1039/d3ra01931d
rsc.li/rsc-advances

1. Introduction

C-Mesenchymal epithelial transition factor (c-Met) is a tyrosine kinase receptor encoded by the proto-oncogene *MET*. It is a high-affinity receptor for hepatocyte growth factor (HGF).¹ When HGF binds to c-Met, it causes c-Met to dimerize, resulting in the phosphorylation of numerous tyrosine residues, which activates a number of intricate signalling pathways involved in cell growth, differentiation, migration, apoptosis, induction of cell polarity, scattering, angiogenesis and invasion.²⁻⁴ Accordingly,

dysregulation of c-Met/HGF signalling pathways that occurred due to abnormal c-Met expression or their stimulation *via* mutation, amplification, translocation, or HGF stimulation were confirmed to be related to the development and/or progression of a wide range of human cancers.^{5,6} Recently, the pharmacological inhibition of c-Met activity is considered as one of the most important strategic pathways in cancer therapy.⁷⁻⁹

Many biological studies have exhibited that there are two groups of c-Met kinase inhibitors based on their structural features and their binding modes with the active site: group I inhibitors and group II inhibitors.¹⁰⁻¹² The inhibitors of type I are ATP analogues and compete with ATP to bind to the extremely conservative hinge region of c-Met kinase. On the other hand, type II inhibitors interact with the same region as type I inhibitors and interact with the allosteric site located beyond the entrance of the active site of c-Met *via* hydrogen and hydrophobic bindings. According to recent reports, some mutations close to the c-Met active site may result in type I inhibitor resistance. Consequently, type II inhibitors may be more successful than type I inhibitors against mutations close to the c-Met active site due to their multi-binding nature.^{2,13-15} Fig. 1 exhibits different compounds possessing different

^aDepartment of Chemistry, Faculty of Science, King Abdulaziz University, P.O. Box 42805, Jeddah 21551, Saudi Arabia

^bDepartment of Chemistry, Faculty of Science, Al-Azhar University, Assiut 71524, Egypt

^cDepartment of Therapeutic Chemistry, National Research Centre, Dokki, Cairo 12622, Egypt. E-mail: manal.hasan52@live.com

^dDepartment of Pharmaceutical Medicinal Chemistry and Drug Design, Faculty of Pharmacy (Girls), Al-Azhar University, Cairo 11754, Egypt. E-mail: dr.emannossier@gmail.com

^eThe National Committee of Drugs, Academy of Scientific Research and Technology, Cairo, 11516, Egypt

† Electronic supplementary information (ESI) available. See DOI: <https://doi.org/10.1039/d3ra01931d>



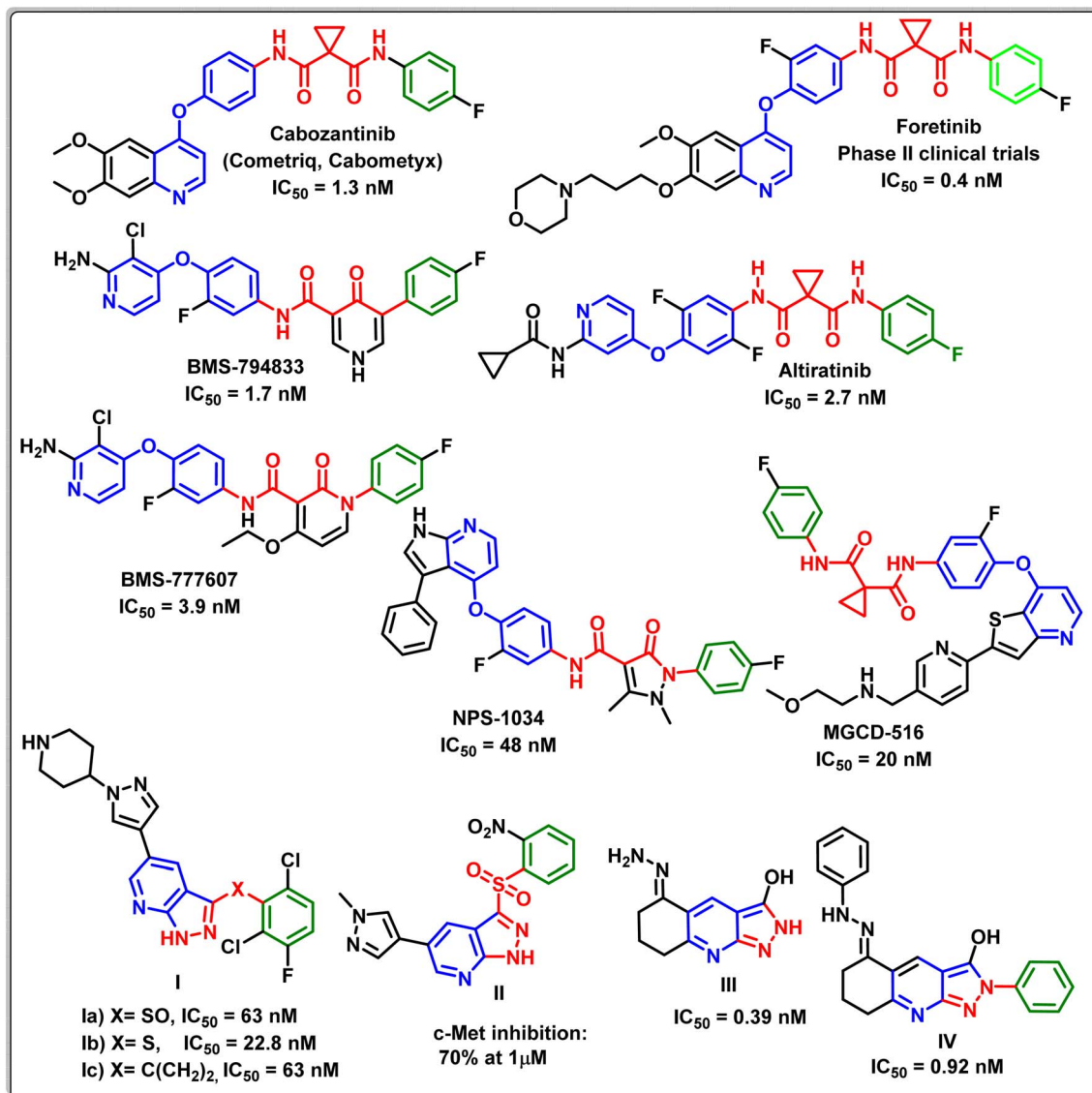


Fig. 1 Different examples of type II c-Met inhibitors bearing different scaffolds.

scaffolds as type II c-Met inhibitors, where some of them have been launched or are in clinical trials.^{16–22}

Recent studies showed that the structures of type II c-Met inhibitors can be divided into three units (A–C).¹³ Unit A of c-Met inhibitors is usually a phenyl or *p*-substituted phenyl moiety, which generates hydrophobic interactions with the hydrophobic pocket of the c-Met protein. Unit B is a linker bridge that could be a linear chain or a heterocyclic ring and should possess hydrogen-bond donors or acceptors. On the other hand, unit C exhibits a high degree of structural diversity, such as pyridine or its analogues attached to a different substituted phenyl moiety, resulting in the creation of hydrogen bonds and π – π stacking interactions with the backbone of the c-Met enzyme^{23–25} (Fig. 2).

Considered one of the most promising privileged scaffolds is pyrazolo[3,4-*b*]pyridine. Many small compounds with pyrazolo[3,4-*b*]pyridine bases have demonstrated a clinical value in a number of medical research disciplines. It is interesting to

note that pyrazolo[3,4-*b*]pyridine derivatives have been linked to a wide range of pharmacological actions.²⁶

Of particular interest, the anticancer activity of pyrazolo[3,4-*b*]pyridines is one of the most significant pharmacological actions. It has been reported that the pyrazolo[3,4-*b*]pyridine derivatives can exert their antitumor impact *via* various mechanisms such as cell growth inhibition,²⁷ apoptosis induction,²⁸ angiogenesis inhibition²⁹ as well as by targeting diverse tyrosine, serine/threonine and lipid kinases including for example adenosine 5'-monophosphate-activated protein kinase (AMPK),³⁰ B-Raf kinase,^{31,32} epidermal growth factor receptor kinase (EGFR),³² checkpoint kinase 1 (CHK1),³³ c-Met kinase,³⁴ fibroblast growth factor receptor (FGFR),³⁵ PIM-1 kinase,³⁶ glycogen synthase kinase-3 (GSK-3),³⁷ and cyclin-dependent kinases (CDKs).³⁸

Liu *et al.*,³⁹ have designed and synthesized new pyrazolo[3,4-*b*]pyridine derivatives **Ia–c**, with a sulfoxide, sulfur, and methylene as a linker. The enzyme assay and cell assay *in vitro* exhibited the strong c-Met kinase inhibitory activity of the latter



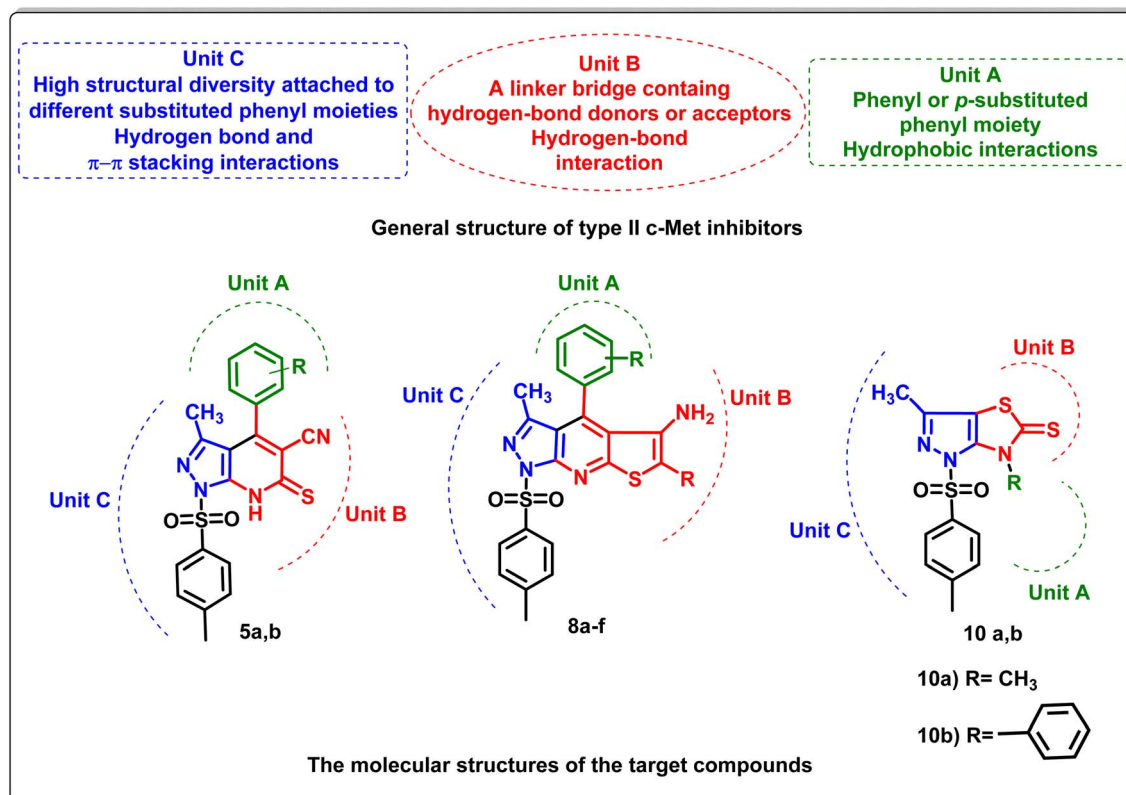


Fig. 2 The design strategy and the molecular structures of the new target derivatives.

derivatives with IC_{50} values in the nano range. Also Ma *et al.*⁴⁰ have synthesized the metabolically stable pyrazolo[3,4-*b*]pyridine derivative **II**, which inhibited c-Met at concentration of 1 μ M. Furthermore, it has been reported that both compounds **III** and **IV** exhibited potent c-Met inhibitory activity of IC_{50} values of 0.39 and 0.92 nM, respectively.⁴¹

Cancer continues to be a major public health concern on a global scale.^{42,43} Over 10 million people die from cancer each year, and the number of cases has increased dramatically worldwide. Although surgery, chemotherapy, and radiation (RT) are currently the primary methods for treating cancer, there have been many instances in which these therapies have had serious negative effects on healthy tissues or have failed to prevent tumor spread or recurrence.^{44,45} Accordingly, with the aim of exploring new effective type II c-Met inhibitors with minimal side effects and based on the structure–activity relationships (SARs) and structural characteristic pharmacophores mentioned earlier, 1-tosyl-pyrazolo[3,4-*b*]pyridine fragments were introduced into block C aiming to create hydrogen bonds and π - π stacking interaction with c-Met backbone and different substituents were tested on block A to evaluate their influences on the c-Met inhibitory activity. The linker bridge which is a part of the heterocyclic pyridine ring (NH-CS-C-CN) in block B was retained to form vital hydrogen bonds with the receptor residues.

Several studies have found that the thiazole heterocycle has intriguing anti-cancer activity against various human cancer cells *via* diverse mechanisms such as apoptosis, DNA intercalation, and enzyme inhibition, including epidermal growth

factor receptors and B-RAF kinase.^{47–50} Thus, bioisostere replacement of the pyrazolo[3,4-*b*]pyridine scaffold with the pyrazolo[3,4-*d*]thiazole scaffold was also studied to see how it affected anticancer and c-Met inhibitory activity.

All the target compounds were evaluated against three cancer cell lines; the liver cancer cell line (HepG-2), breast cancer cell line (MCF-7), and colorectal cancer cell line (HCT), in addition to their cytotoxic activity against the normal WI-38 cell line. The most promising candidates were further assessed as c-Met kinase inhibitors. Extra investigations were also carried out to investigate the mechanistic pathways of the antiproliferative activity of the most potent compounds, such as cell cycle analysis, apoptosis, and the impacts of these derivatives on the oncogenic markers; Bax, Bcl-2, p53, and caspase-3. Moreover, molecular docking research was carried out on the most potent c-Met inhibitors to highlight and justify their modes of action. *In silico* ADMET prediction was also performed for the potent compounds to investigate their drug-likeness characteristics.

2. Experimental

2.1. Chemistry

The instrumental devices used for measuring the melting points, spectral data (IR, Mass, ¹H NMR and ¹³C NMR) and elemental analyses are provided in details in ESI.†

2.1.1. General procedure for the synthesis of thioxopyrazolo[3,4-*b*]pyridine derivatives 5a,b. A mixture of 3-methyl-1-tosyl-1*H*-pyrazol-5(4*H*)-one (**1**) (10 mmol) and different arylidine



cyanothioacetamide derivatives (10 mmol) in absolute ethanol (30 mL) containing a catalytic amount of piperidine (0.5 mL) was heated under reflux for 7 h. Then the reaction mixture was cooled, poured onto crushed ice and acidified with HCl. The obtained solid product was collected by filtration and recrystallized from ethanol to afford the target compounds **5a,b**.

2.1.1.1. 3-Methyl-4-phenyl-6-thioxo-1-tosyl-6,7-dihydro-1*H*-pyrazolo[3,4-*b*]pyridine-5-carbonitrile (5a). Yield: 88%; yellow crystals; mp 222–224 °C; FT-IR (KBr) ($\nu_{\text{max}}/\text{cm}^{-1}$): 3306 (NH), 3058 (CH-aromatic), 2979 (CH-aliphatic), 2215 (CN); ^1H NMR (300 MHz, DMSO- d_6) δ = 2.24 (s, 3H, CH₃), 2.36 (s, 3H, CH₃), 7.32–7.86 (m, 9H, Ar-H), 11.76 (s, 1H, NH, D₂O exchangeable); ^{13}C NMR (100 MHz, DMSO- d_6) δ : 14.1 (CH₃), 22.4 (CH₃), 101.9, 106.7, 115.6, 127.1, 128.1, 128.2, 128.7, 131.8, 134.8, 137.9, 140.4, 140.7, 151.9, 162.9 (Ar-C), 179.6 (C=S); EI-MS m/z (%): 476 [M⁺] (35.31); anal. calcd for C₂₄H₂₀N₄O₃S₂ (476.57): C, 60.49; H, 4.23; N, 11.76; S, 13.46%; found: C, 60.71; H, 4.45; N, 11.54; S, 13.67%.

2.1.1.2. 4-(4-Chlorophenyl)-3-methyl-6-thioxo-1-tosyl-6,7-dihydro-1*H*-pyrazolo[3,4-*b*]pyridine-5-carbonitrile (5b). Yield: 85%; yellow crystals; mp 217–219 °C; FT-IR (KBr) ($\nu_{\text{max}}/\text{cm}^{-1}$): 3340 (NH), 3054 (CH-arom.), 2943 (CH-aliph.), 2208 (CN); ^1H NMR (300 MHz, DMSO- d_6) δ = 2.33 (s, 3H, CH₃), 2.62 (s, 3H, CH₃), 6.76–6.87 (2d, J = 7.5 Hz, 2H, Ar-H), 7.05–7.08 (2d, J = 7.5 Hz, 2H, Ar-H), 7.41–7.43 (2d, J = 7.5 Hz, 2H, Ar-H), 7.81–7.84 (2d, J = 7.5 Hz, 2H, Ar-H), 11.58 (s, 1H, NH, D₂O exchangeable); ^{13}C NMR (100 MHz, DMSO- d_6) δ : 12.1 (CH₃), 21.8 (CH₃), 100.2, 108.2, 115.1, 126.1, 127.7, 128.3, 130.4, 133.5, 134.1, 136.0, 138.1, 140.3, 149.5, 161.3 (Ar-C), 178.5 (C=S); EI-MS m/z (%): 4454 [M⁺] (30.21); anal. calcd for C₂₁H₁₅Cl N₄O₂S₂ (454.95): C, 55.44; H, 3.32; Cl, 7.79; N, 12.31; S, 14.10%; found: C, 55.32; H, 3.54; Cl, 7.58; N, 12.53; S, 14.31%.

2.1.2. General procedure for the synthesis of compounds 8a–f. A mixture of thioxopyrazolo[3,4-*b*]pyridine derivatives **5a,b** (10 mmol), various halo compounds such as, 2-chloroacetamide, 1-chloropropan-2-one, 2-chloroacetonitrile, ethyl 2-chloroacetate, and 2-chloroacetic (**6a–e**) (10 mmol), and sodium ethoxide (10 mmol) in absolute ethanol (30 mL) was heated under reflux for 9 h. The reaction mixture was left to cool, poured onto cold water, and acidified with HCl. The solid product formed was collected by filtration and recrystallized from ethanol/dioxane to afford the target compounds **8a–f**.

2.1.2.1. 5-Amino-3-methyl-4-phenyl-1-tosyl-1*H*-pyrazolo[3,4-*b*]thieno[3,2-*e*]pyridine-6-carboxamide (8a). Yield: 67%; yellow crystals; mp 272–274 °C; FT-IR (KBr) ($\nu_{\text{max}}/\text{cm}^{-1}$): 3422, 3339, 3315, 3148 (2NH₂), 3081 (CH-aromatic), 2921 (CH-aliphatic), 1680 (C=O); ^1H NMR (300 MHz, DMSO- d_6) δ : 2.02 (s, 3H, CH₃), 2.26 (s, 3H, CH₃), 5.92 (s, 2H, NH₂, D₂O exchangeable), 6.83–7.84 (m, 11H, Ar-H + NH₂); ^{13}C NMR (100 MHz, DMSO- d_6) δ : 13.5 (CH₃), 21.6 (CH₃), 110.1, 122.3, 124.0, 126.0, 126.9, 127.7, 129.4, 130.5, 130.9, 134.5, 134.8, 138.1, 138.7, 155.7, 159.2 (aromatic-C), 164.6 (C=O); EI-MS m/z (%): 477 [M⁺] (30.51); anal. calcd for C₂₃H₁₉N₅O₃S₂ (477.56): C, 57.85; H, 4.01; N, 14.66; S, 13.43%; found: C, 57.63; H, 4.22; N, 14.87; S, 13.65%.

2.1.2.2. 1-(5-Amino-3-methyl-4-phenyl-1-tosyl-1*H*-pyrazolo[3,4-*b*]thieno[3,2-*e*]pyridin-6-yl)ethan-1-one (8b). Yield: 70%;

yellow crystals; mp 287–289 °C; FT-IR (KBr) ($\nu_{\text{max}}/\text{cm}^{-1}$): 3421, 3279 (NH₂), 3030 (CH-aromatic), 2952 (CH-aliphatic), 1692 (C=O); ^1H NMR (300 MHz, DMSO- d_6) δ : 2.06 (s, 3H, CH₃), 2.22 (s, 3H, CH₃), 2.63 (s, 3H, CH₃), 6.38 (s, 2H, NH₂, D₂O exchangeable), 7.20–7.71 (m, 9H, Ar-H); ^{13}C NMR (100 MHz, DMSO- d_6) δ : 15.8 (CH₃), 22.1 (CH₃), 25.5 (CH₃), 111.3, 120.1, 124.1, 124.3, 128.6, 128.7, 129.5, 133.8, 133.9, 135.0, 135.7, 139.7, 142.3, 148.2, 157.7, 157.9 (aromatic-C), 182.4 (C=O); EI-MS m/z (%): 476 [M⁺] (35.31); anal. calcd for C₂₄H₂₀N₄O₃S₂ (476.57): C, 60.49; H, 4.23; N, 11.76; S, 13.46%; found: C, 60.71; H, 4.45; N, 11.54; S, 13.67%.

2.1.2.3. 5-Amino-4-(4-chlorophenyl)-3-methyl-1-tosyl-1*H*-pyrazolo[3,4-*b*]thieno[3,2-*e*]pyridine-6-carbonitrile (8c). Yield: 71%; yellow crystals; mp 276–278 °C; FT-IR (KBr) ($\nu_{\text{max}}/\text{cm}^{-1}$): 3405, 3319 (NH₂), 3057 (CH-aromatic), 2965 (CH-aliphatic), 2220 (CN); ^1H NMR (300 MHz, DMSO- d_6) δ : 2.12 (s, 3H, CH₃), 2.35 (s, 3H, CH₃), 6.45 (s, 2H, NH₂, D₂O exchangeable), 7.14–7.17 (2d, J = 7.5 Hz, 2H, Ar-H), 7.21–7.24 (2d, J = 7.5 Hz, 2H, Ar-H), 7.33–7.35 (2d, J = 7.5 Hz, 2H, Ar-H), 7.53–7.55 (2d, J = 7.5 Hz, 2H, Ar-H); ^{13}C NMR (100 MHz, DMSO- d_6) δ : 11.6 (CH₃), 25.0 (CH₃), 102.3, 107.9, 113.6, 121.0, 126.9, 127.9, 128.7, 130.4, 130.8, 133.4, 133.9, 136.5, 138.1, 142.1, 149.4, 156.1, 159.5 (aromatic-C); EI-MS m/z (%): 493 [M⁺] (30.31); anal. calcd for C₂₃H₁₆Cl N₅O₂S₂ (493.99): C, 55.92; H, 3.26; Cl, 7.18; N, 14.18; S, 12.98%; found: C, 55.70; H, 3.74; Cl, 7.39; N, 14.38; S, 12.76%.

2.1.2.4. Ethyl 5-amino-4-(4-chlorophenyl)-3-methyl-1-tosyl-1*H*-pyrazolo[3,4-*b*]thieno[3,2-*e*]pyridine-6-carboxylate (8d). Yield: 72%; yellow crystals; mp 267–269 °C; FT-IR (KBr) ($\nu_{\text{max}}/\text{cm}^{-1}$): 3346, 2294 (NH₂), 3068 (CH-aromatic), 2976 (CH-aliphatic), 1720 (C=O); ^1H NMR (300 MHz, DMSO- d_6) δ : 1.28 (t, J = 7.5 Hz, 3H, OCH₂CH₃), 2.04 (s, 3H, CH₃), 2.47 (s, 3H, CH₃), 4.27 (q, J = 7.5 Hz, 2H, OCH₂CH₃), 6.24 (s, 2H, NH₂, D₂O exchangeable), 6.92–6.94 (2d, J = 7.5 Hz, 2H, Ar-H), 7.32–7.35 (2d, J = 7.5 Hz, 2H, Ar-H), 7.50–7.53 (2d, J = 7.5 Hz, 2H, Ar-H), 7.54–7.57 (2d, J = 7.5 Hz, 2H, Ar-H); ^{13}C NMR (100 MHz, DMSO- d_6) δ : 12.2 (OCH₂CH₃), 12.6 (CH₃), 22.7 (CH₃), 60.2 (OCH₂CH₃), 110.3, 119.1, 123.7, 126.8, 127.9, 129.4, 130.6, 130.7, 134.3, 134.8, 136.5, 138.8, 146.2, 153.1 (aromatic-C), 160.7 (C=O); EI-MS m/z (%): 541 [M⁺] (45.25); anal. calcd for C₂₅H₂₁ClN₄O₄S₂ (541.04): C, 55.50; H, 3.91; Cl, 6.55; N, 10.36; S, 11.85%; found: C, 55.71; H, 3.69; Cl, 6.77; N, 10.58; S, 11.64%.

2.1.2.5. 1-(5-Amino-4-(4-chlorophenyl)-3-methyl-1-tosyl-1*H*-pyrazolo[3,4-*b*]thieno[3,2-*e*]pyridin-6-yl)ethan-1-one (8e). Yield: 65%; yellow crystals; mp 281–283 °C; FT-IR (KBr) ($\nu_{\text{max}}/\text{cm}^{-1}$): 3423, 3371 (NH₂), 3028 (CH-aromatic), 2981 (CH-aliphatic), 1685 (C=O); ^1H NMR (300 MHz, DMSO- d_6) δ : 2.19 (s, 3H, CH₃), 2.32 (s, 3H, CH₃), 2.78 (s, 3H, CH₃), 6.25 (s, 2H, NH₂, D₂O exchangeable), 7.02–7.04 (2d, J = 7.5 Hz, 2H, Ar-H), 7.19–7.21 (2d, J = 7.5 Hz, 2H, Ar-H), 7.42–7.44 (2d, J = 7.5 Hz, 2H, Ar-H), 7.65–7.68 (2d, J = 7.5 Hz, 2H, Ar-H); ^{13}C NMR (100 MHz, DMSO- d_6) δ : 16.7 (CH₃), 22.1 (CH₃), 27.1 (CH₃), 111.0, 120.9, 124.1, 127.7, 127.9, 133.3, 133.6, 135.9, 136.8, 137.01, 137.04, 140.7, 144.7, 156.0, 158.8 (aromatic-C), 181.8 (C=O); EI-MS m/z (%): 511 [M⁺] (35.11); anal. calcd for C₂₄H₁₉ClN₄O₃S₂ (511.02): C, 56.41; H, 3.75; Cl, 6.94; N, 10.96; S, 12.55%; found: C, 56.63; H, 3.95; Cl, 6.73; N, 10.75; S, 12.78%.



2.1.2.6. 5-Amino-4-(4-chlorophenyl)-3-methyl-1-tosyl-1*H*-pyrazolo[3,4-*b*]thieno[3,2-*e*]pyridine-6-carboxylic acid (8f). Yield: 62%; yellow crystals; mp 264–266 °C; FT-IR (KBr) (ν_{max} /cm^{−1}): 3455 (OH), 3406, 3390 (NH₂), 3057 (CH-aromatic), 2928 (CH-aliphatic), 1688 (C=O); ¹H NMR (300 MHz, DMSO-*d*₆) δ : 2.03 (s, 3H, CH₃), 2.37 (s, 3H, CH₃), 6.29 (s, 2H, NH₂, D₂O exchangeable), 6.85–6.87 (2d, *J* = 7.2 Hz, 2H, Ar-H), 7.04–7.06 (2d, *J* = 7.2 Hz, 2H, Ar-H), 7.72–7.74 (2d, *J* = 7.2 Hz, 2H, Ar-H), 7.83–7.85 (2d, *J* = 7.2 Hz, 2H, Ar-H), 11.78 (s, 1H, OH, D₂O exchangeable); ¹³C NMR (100 MHz, DMSO-*d*₆) δ : 12.0 (CH₃), 20.1 (CH₃), 110.4, 118.3, 123.3, 127.6, 27.7, 128.5, 130.1, 131.2, 131.9, 135.7, 139.75, 139.76, 142.3, 156.2, 158.6 (aromatic-C), 165.5 (C=O); EI-MS *m/z* (%): 512 [M⁺] (40.25); anal. calcd for C₂₃H₁₇ClN₄O₄S₂ (512.99): C, 53.85; H, 3.34; Cl, 6.91; N, 10.92; S, 12.50%; found: C, 53.64; H, 3.56; Cl, 6.70; N, 10.69; S, 12.73%.

2.1.3. General procedure for synthesis of pyrazolo[3,4-*d*]thiazole-5-thiones 10a,b. A mixture of the pyrazolone derivative 1 (10 mmol), different isothiocyanate derivatives 9a,b (10 mmol), elemental sulfur (10 mmol), and dimethylformamide (2 mL) in absolute ethanol (30 mL) containing a few drops of triethylamine was heated under reflux for 9 h. After cooling, the reaction mixture was acidified by HCl, and the solid product formed in each case was collected by filtration and recrystallized from ethanol/DMF.

2.1.3.1. 3,6-Dimethyl-1-tosyl-1,6-dihydro-5*H*-pyrazolo[3,4-*d*]thiazole-5-thione (10a). Yield: 59%; brown crystals; mp 291–293 °C; FT-IR (KBr) (ν_{max} /cm^{−1}): 3037 (CH-aromatic), 2972 (CH-aliphatic), 1276 (C=S); ¹H NMR (300 MHz, DMSO-*d*₆) δ : 2.18 (s, 3H, CH₃), 2.37 (s, 3H, CH₃), 2.99 (s, 3H, CH₃), 7.23–7.25 (2d, *J* = 7.2 Hz, 2H, Ar-H), 7.79–7.81 (2d, *J* = 7.2 Hz, 2H, Ar-H); ¹³C NMR (100 MHz, DMSO-*d*₆) δ : 17.8 (CH₃), 21.6 (CH₃), 31.5 (CH₃), 102.2, 127.1, 130.0, 134.5, 136.3, 137.8, 143.4, 154.6 (aromatic-C), 182.1 (C=S); EI-MS *m/z* (%): 339 [M⁺] (30.29); anal. calcd for C₁₃H₁₃N₃O₂S₃ (339.46): C, 46.00; H, 3.86; N, 12.38; S, 28.34%; found: C, 46.21; H, 3.64; N, 12.59; S, 28.57%.

2.1.3.2. 3-Methyl-6-phenyl-1-tosyl-1*H*-pyrazolo[3,4-*d*]thiazole-5(6*H*)-thione (10b). Yield: 61%; brown crystals; mp 295–297 °C; FT-IR (KBr) (ν_{max} /cm^{−1}): 3045 (CH-aromatic), 2964 (CH-aliphatic), 1273 (C=S); ¹H NMR (300 MHz, DMSO-*d*₆) δ : 2.01 (s, 3H, CH₃), 2.82 (s, 3H, CH₃), 7.05–7.89 (m, 9H, Ar-H); ¹³C NMR (100 MHz, DMSO-*d*₆) δ : 10.3 (CH₃), 23.7 (CH₃), 101.5, 127.3, 127.7, 128.01, 128.04, 130.8, 132.1, 132.4, 138.2, 140.2, 155.0 (aromatic-C), 180.1 (C=S); anal. calcd for C₁₈H₁₅N₃O₂S₃ (401.53): C, 53.84; H, 3.77; N, 10.47; S, 23.96%; found: C, 53.63; H, 3.56; N, 10.68; S, 23.73%.

2.2. Biological assays

2.2.1. *In vitro* anticancer screening. The anticancer activity of the new compounds was screened using MTT assay at Regional Center for Mycology and Biotechnology, Al-Azhar University. More details are provided in ESI.†

2.2.2. c-Met kinase inhibitory assay. The c-Met kinase activity was determined in 384-well plates using homogenous time-resolved fluorescence (HTRF) assays following the manufacturer's instruction. More details are provided in ESI.†

2.2.3. Cell cycle analysis. HepG-2 cell line was treated with the most potent compound 5a at its IC₅₀ concentration for 24 h. More details are provided in ESI.†

2.2.4. Apoptosis assay. Annexin V-FITC apoptosis detection kit (BD Biosciences) was used to quantify the percentage of cells undergoing apoptosis and to detect the modes of cell death either by apoptosis or necrosis. More details are provided in ESI.†

2.2.5. Estimation of Bax and Bcl-2 levels. Quantitative determination of pro-apoptotic BAX and anti-apoptotic Bcl-2 proteins in human cell lysates was performed using DRG® Human Bax ELISA (EIA-4487) and Zymed® Bcl-2 ELISA Kit (99-0042). More details are provided in ESI.†

2.2.6. Estimation of human p53 level. Human p53 present in HepG-2 cells was determined; using Human p53 ELISA-Kit (CS0070 Sigma) read using spectrophotometer at 450 nm. More details are provided in ESI.†

2.2.7. Human CASP-3 (caspase-3) estimation. Antibody-substrate intensity is measured spectrophotometrically to weight up the caspase protein quantity. More details are provided in ESI.†

2.3. Computational studies

2.3.1. Molecular docking study. The molecular docking simulation of the promising *in vitro* screened derivatives 5a and 5b against c-Met was done using the Molecular Operating Environment software (MOE-Dock) version 2014.0901. More details are provided in ESI.†

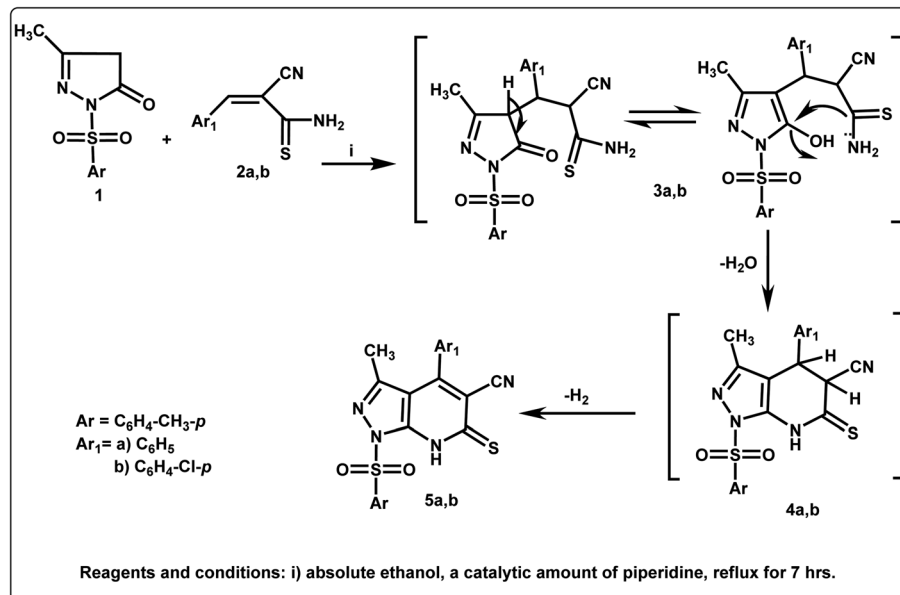
2.3.2. *In silico* ADME prediction study. Concerning the described approach, the highly effective the 6-thioxopyrazolo[3,4-*b*]pyridine-5-carbonitrile targets 5a and 5b were further examined for their predictable physicochemical and pharmacokinetic characteristics using the free web tool, SwissADME. More details are provided in ESI.†

3. Results and discussion

3.1. Chemistry

The new target compounds were synthesized according to the synthetic pathways outlined in Schemes 1–3. Their structures were confirmed based on their elemental analyses and spectral data (ESI†). According to Scheme 1, the starting compound 3-methyl-1-tosyl-1*H*-pyrazol-5(4*H*)-one (1) was condensed with different arylidene cyanothioacetamide derivatives, namely, 2-cyano-3-phenylprop-2-enethioamide and 3-(4-chlorophenyl)-2-cyanoprop-2-enethioamide 2a and 2b, respectively, in absolute ethanol containing a catalytic amount of piperidine, as a basic medium to afford the corresponding thioxopyrazolo[3,4-*b*]pyridines 5a,b (Scheme 1). IR spectra of compounds 5a,b were characterized by the appearance of absorption peaks in the ranges 3340–3306 and 2215–2208 cm^{−1} related to NH and CN groups, respectively. Also, ¹H NMR spectra of 5a,b showed singlet signals at δ = 2.24–2.70 ppm attributed to the CH₃ moieties, the appearance of different multiplet signals at δ = 6.70–7.86 ppm related to the aromatic protons, and a D₂O exchangeable singlet signal at δ = 11.58–11.76 ppm assignable



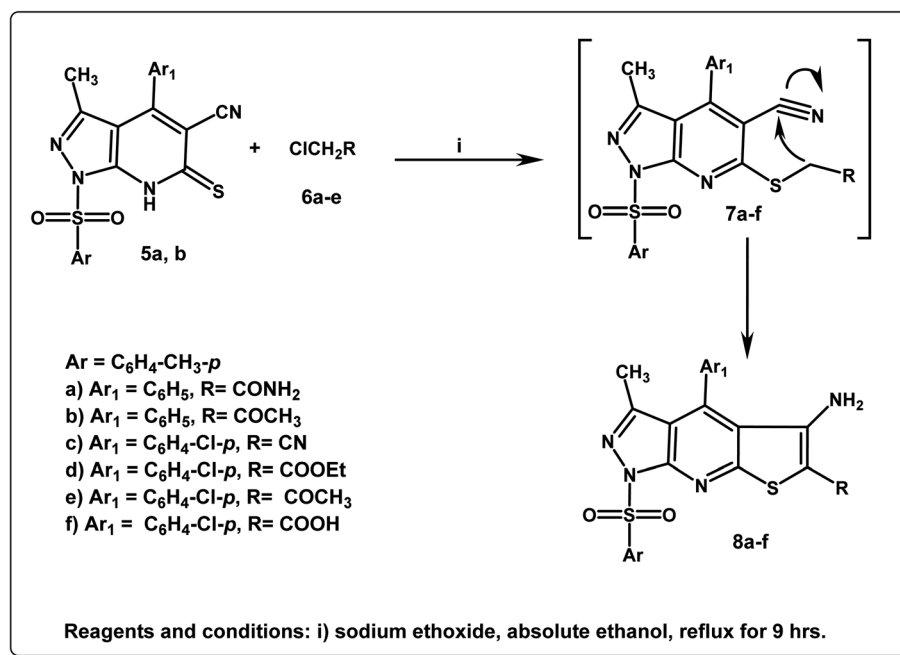


Scheme 1 Synthetic approach of thioxopyrazolo[3,4-b]pyridine derivatives 5a,b.

to the NH group. In addition, ^{13}C NMR spectra of 5a,b exhibited the two methyl groups as two singlets at $\delta = 12.1\text{--}22.4$ ppm, the aromatic carbons as singlet signals in the region $\delta = 100.2\text{--}163.0$ ppm, whereas C=S group appeared as a singlet signal at 178.5–179.6 ppm.

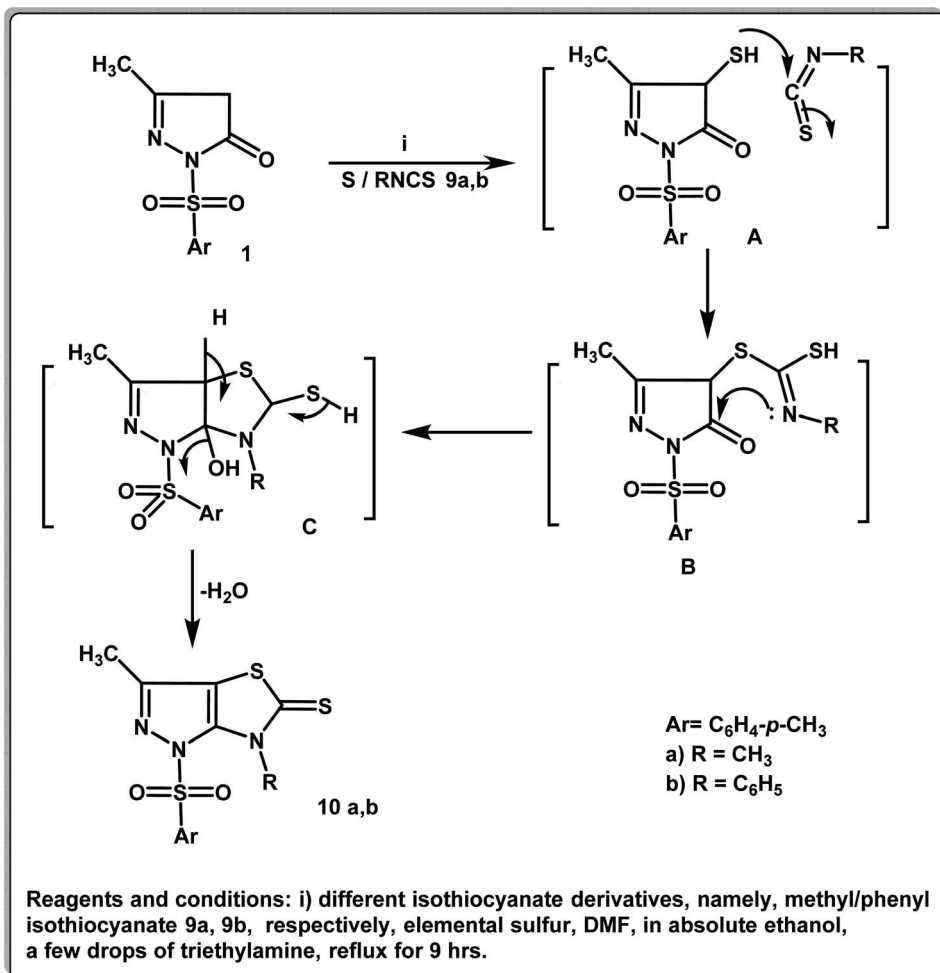
In addition, Scheme 2 depicts the cyclo-condensation of the thioxopyrazolo[3,4-b]pyridines 5a,b with various alkyl halides, such as 2-chloroacetamide, 1-chloropropan-2-one, 2-chloroacetonitrile, ethyl 2-chloroacetate, and 2-chloroacetic, in absolute ethanol containing sodium ethoxide, leading to the

formation of the three corresponding cyclic pyrazolo[3,4-b]thieno[3,2-e]pyridine compounds 8a-f. The proposed mechanistic route for the formation of the latter derivatives 8a-f involves the nucleophilic attack of the thiol group (–SH) of compounds 5a,b on the used halogen compounds, followed by the elimination of the HCl molecule to yield the non-isolated intermediates 7a-f, which were then cyclized to yield the final products 8a-f. IR spectra of the target derivatives 8a-f displayed various absorption stretching bands in the region 3405–3352 cm^{-1} corresponding to the NH₂ groups and at 2221 cm^{-1}



Scheme 2 Synthetic approach of pyrazolo[3,4-b]thieno[3,2-e]pyridine derivatives 8a-f.





Scheme 3 Synthetic approach of pyrazolo[3,4-d]thiazole-5-thione derivatives 10a,b.

due to CN group of the compound **8c**. Furthermore, ¹H NMR spectra of **8a-f** revealed the protons of the parent groups (CH₃, aromatic, and NH₂) in their expected regions in addition to a singlet signal at δ 2.78 ppm due to 6-CH₃ of compounds **8b** and **8e**. The characteristic triplet-quartet signals of OCH₂-CH₃ of compound **8d** appeared at δ 1.20, and 4.13 ppm. ¹³C NMR spectra of the derivatives **8a-f** illustrated signals at δ 11.6-25.0 ppm due to CH₃ functionalities and at δ 110.0-148.2 ppm due to the aromatic carbons. Also, the compounds **8a,b** and **8d-f** revealed singlet signals in the range δ 160.7-181.8 ppm referring to C=O groups. Compound **8d** exhibited an additional singlet at δ 60.2 ppm assignable to the methylene carbon of OCH₂CH₃ group (Scheme 2).

Utilizing Hantzsch reaction for thiazole synthesis led to the formation of the corresponding pyrazolo[3,4-d]thiazole-5-thione derivatives **10a,b**. The reaction was carried out *via* the treatment of 3-methyl-1-tosyl-1*H*-pyrazol-5(4*H*)-one (**1**) with elemental sulfur and methyl/phenylisothiocyanate in dimethylformamide/ethanol solution containing a few drops of triethylamine.

¹H NMR spectra of **10a,b** revealed the protons of the parent groups (2CH₃ and aromatic protons) in their expected regions

in addition to a singlet signal at δ 2.99 ppm due to N-CH₃ of compound **10a**. Moreover, ¹³C NMR spectra of the derivatives **10a,b** illustrated singlet signals in the regions δ 10.3-31.5 ppm due to CH₃ moieties, δ 101.0-155.0 ppm referring to the aromatic carbons and δ 180.0.1-182.2 ppm referring to C=S groups (Scheme 3).

The mass spectra of all new compounds represented molecular ion peaks which were in agreement with molecular formulae.

3.2. Biological activity

3.2.1. In vitro cytotoxic activity. Overexpression of the c-Met protein has been investigated in many types of cancer cells, such as breast cancer,⁴⁵ non-small-cell lung cancer (NSCLC),⁴⁶ gastric cancer,⁴⁷ head and neck cancer,⁴⁸ cervix cancer,⁴⁹ pancreatic cancer,⁵⁰ hepatocellular carcinoma (HCC),⁵¹ renal cell carcinoma (RCC),⁵² and colorectal cancer.⁵³ In this research, all the target compounds were assessed in terms of antiproliferative activity against three human cancer cell lines with high expression of c-Met protein, including the liver cancer cell line (HepG-2), breast cancer cell line (MCF-7), and colorectal cancer cell line (HCT), utilizing the colorimetric MTT assay.^{54,55}

Table 1 The antitumor activities of the target compounds against HepG-2, MCF-7, HCT-116, and WI-38 cancer cell lines expressed as IC₅₀ values

Tested compounds	IC ₅₀ values ^a (μM) against tumor cell lines			
	HepG-2	MCF-7	HCT-116	WI-38
5a	3.42 ± 1.31 (SI = 23.52)	5.25 ± 1.04 (SI = 15.32)	6.27 ± 1.15 (SI = 12.83)	80.46 ± 0.33
5b	3.56 ± 1.5 (SI = 23.90)	6.82 ± 1.1 (SI = 12.47)	9.21 ± 0.02 (SI = 9.23)	85.10 ± 0.32
8a	30.58 ± 0.01	43.02 ± 0.24	47.38 ± 0.11	
8b	52.08 ± 0.71	60.23 ± 0.17	67.84 ± 0.02	
8c	25.37 ± 0.5	36.25 ± 0.13	41.77 ± 0.4	
8d	23.12 ± 0.08	32.14 ± 0.19	38.11 ± 0.3	
8e	12.31 ± 0.1	14.18 ± 0.33	18.21 ± 0.62	
8f	15.44 ± 0.3	19.27 ± 0.45	18.86 ± 0.12	
10a	10.23 ± 0.15	13.65 ± 0.7	17.16 ± 0.37	
10b	6.75 ± 0.62 (SI = 12.65)	8.13 ± 0.4 (SI = 10.50)	9.36 ± 0.45 (SI = 9.12)	85.41 ± 0.51
5-Fluorouracil	2.87 ± 0.15 (SI = 27.77)	3.58 ± 0.45 (SI = 22.26)	5.26 ± 0.31 (SI = 15.15)	79.70 ± 0.64
Erlotinib	8.19 ± 0.4 (SI = 2.94)	4.16 ± 0.2 (SI = 5.79)	7.41 ± 1.12 (SI = 3.25)	69.99 ± 1.08

^a IC₅₀ values = mean ± SD of three independent determinations.

5-Fluorouracil (5-FU) and erlotinib were assigned as positive controls. The concentrations of the tested compounds that resulted in 50% inhibition of cell viability (IC₅₀, μM) were detected and tabulated in Table 1. It is evident in Table 1 that many compounds displayed moderate to promising cytotoxic potency towards the three tested cell lines, where some of them exhibited equipotent activities against one or more cell lines in comparison with the reference drugs.

As shown in Table 1, the derivatives **5a,b** with a common structural feature of thioxopyrazolo[3,4-*b*]pyridine nucleus exhibited the most growth inhibitory activity against the three examined cell lines with IC₅₀ values ranging from 3.42 ± 1.31 to 9.21 ± 0.02 μM. In comparison to erlotinib, the compound **5a** and its chlorinated analogue **5b** were approximately 2.4-fold more potent against the HepG-2 cancer cell line (IC₅₀ values: 3.42 ± 1.3, 3.56 ± 1.5, respectively; IC₅₀ erlotinib, 8.19 ± 0.40 μM). Both compounds were approximately equipotent or slightly less potent against the other two cancer cell lines (MCF-7 and HCT) representing IC₅₀ values ranging from 4.16 ± 0.2 to 9.21 ± 0.02 μM and IC₅₀ erlotinib, 4.16 ± 0.2 and 7.41 ± 1.12 μM, respectively. Meanwhile, a slight decrease in the target activity was detected by both **5a** and **5b** in comparison with 5-FU, which represented IC₅₀s ranging from 2.87 ± 0.15 to 5.26 ± 0.31 μM. It is evident that the HepG-2 cancer cell line was more sensitive to both compounds **5a** and **5b** than the MCF-7 and HCT-116 cell lines. Moreover, the promising sensitivity of the HepG-2 cancer cell line was maintained by the compound bearing the thioxopyrazolo[3,4-*d*]thiazole structural feature **10b** in comparison with erlotinib with IC₅₀ value of 6.75 ± 0.62 μM, but 2.3-fold less when compared with 5-FU. Moreover, a detectable decrease in the activity of **10b** was also reported against the other two cancer cell lines (MCF-7 and HCT) in comparison to both reference drugs, 5-FU and erlotinib, with IC₅₀ values of 8.13 ± 0.4 and 9.36 ± 0.45 μM, respectively. A detectable reduction in the target potency was detected by the methyl analogue **10a** against the three cancer cell lines (IC₅₀ values: 10.23 ± 0.15, 13.65 ± 0.7, and 17.16 ± 0.37, respectively), in comparison with both

standard drugs. This indicated that the substitution of the thiazolidine ring with a phenyl ring is more favorable for the anticancer activity *via* increasing the lipophilicity of the compound. In addition, the fusion of a thiophene ring to the parent thioxopyrazolo[3,4-*b*]pyridine nucleus resulting in the thioxopyrazolo[3,4-*b*]thieno[3,2-*e*]pyridine derivatives **8a-f** was unfavorable for the anti-proliferative activity producing a significant drop against the three cancer cell lines with IC₅₀ values ranging from 12.31 ± 0.11 to 67.84 ± 0.02 μM. This result could be explained by the increase in the size of the molecule leads to its improper orientation and inadequate fitting of the new molecule in the active site of the target protein.

Consequently, the selectivity profile of the three most promising compounds, **5a**, **5b**, and **10b**, towards cancer cells rather than normal cells was valuable to be examined. Accordingly, the cytotoxic activity of the latter analogues was screened in human lung fibroblasts (WI-38) normal cells utilizing MTT assay. Fortunately, the evaluated compounds were more selective for the tested cancer cells than for the normal cell line WI-38, producing IC₅₀ values, 80.46 ± 0.33, 85.10 ± 0.32, and 85.41 ± 0.51 μM, in comparison with 5-FU and erlotinib of IC₅₀ values of 79.70 ± 0.64 and 69.99 ± 1.08 μM. Based on the previous results, the structural thioxopyrazolo[3,4-*b*]pyridine and thioxopyrazolo[3,4-*d*]thiazole features as compounds **5a**, **5b**, and **10b**, respectively are promising cytotoxic scaffolds with significant selectivity indices against normal cells (Table 1) (Fig. 3). On the other hand, the tricyclic ring system such as the thioxopyrazolo[3,4-*b*]thieno[3,2-*e*]pyridine scaffold of compounds **8a-f** is not preferred for the target anticancer activity.

3.2.2. c-Met inhibitory assay *in vitro*. Encouraged by the obtained results of the *in vitro* anti-proliferative activity assay, the most potent compounds **5a**, and **5b** were selected for further evaluation of their c-Met kinase inhibitory activity using a homogeneous time-resolved fluorescence (HTRF) assay utilizing cabozantinib as a positive control.^{40,41} As summarized in Table 2, compound **5a** was close to or slightly more potent than the reference drug cabozantinib with IC₅₀ values of 4.27 ±



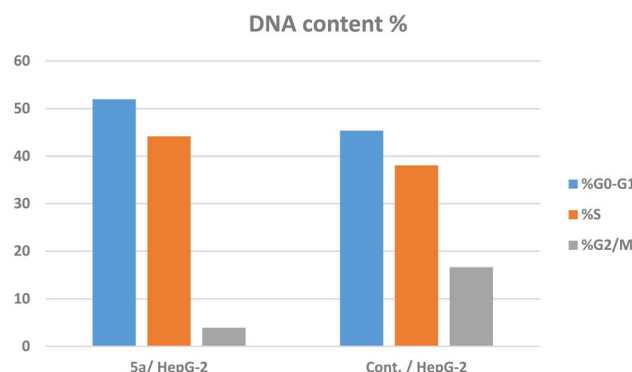


Fig. 3 Cell cycle analysis of 5a in HepG-2 cell line.

Table 2 Inhibitory assessment of the screened compounds 5a and 5b in comparison with cabozantinib against c-Met^a

Compound no.	c-Met	
	IC ₅₀ (mean ± SEM) (nM)	
5a	4.27 ± 0.31	
5b	7.95 ± 0.17	
Cabozantinib	5.38 ± 0.52	

^a IC₅₀: compound concentration required to inhibit the enzyme activity by 50%; SEM: standard error mean; each value is the mean of three values.

0.31 and 5.38 ± 0.52 nM, respectively. On the other hand, the chloro analogue **5b** was slightly less potent than the positive control with IC₅₀ value of 7.95 ± 0.17 nM. The *p*-chlorine atom of the phenyl group might be the reason for devoted **5b** from the proper fitting in the active site of the enzyme resulting in its slight lower inhibitory activity than **5a**.

It could be noted that both compounds showed the most favorable antiproliferation effects and selectivity in the cell assays and also showed promising performance in the enzymatic assay. According to these findings, the pyrazolo[3,4-*b*] pyridine fragment is a privileged scaffold for c-Met inhibitory activity and antiproliferative effect.

3.2.3. Cell cycle arrest induced by compound 5a. The cell cycle is an ordered set of events that results in cell growth and division. The cell cycle is divided into two major phases: interphase and mitosis (M phase). Interphase is subdivided into three subphases: G1, S, and G2. The G1-phase is the first gap phase between the birth of a cell and DNA replication (S phase). The second interphase between DNA replication and cell division is known as the G2 phase. The M-phase is the process of dividing chromosomes into two daughter cells precisely and evenly.^{56,57} Recent studies reported that targeting specific phases of the cell cycle is an effective therapeutic intervention in the management of various antiproliferative diseases.^{58–60} In order to investigate the mechanism underlying the anti-proliferative activity of compound **5a**, cell cycle distribution was studied.

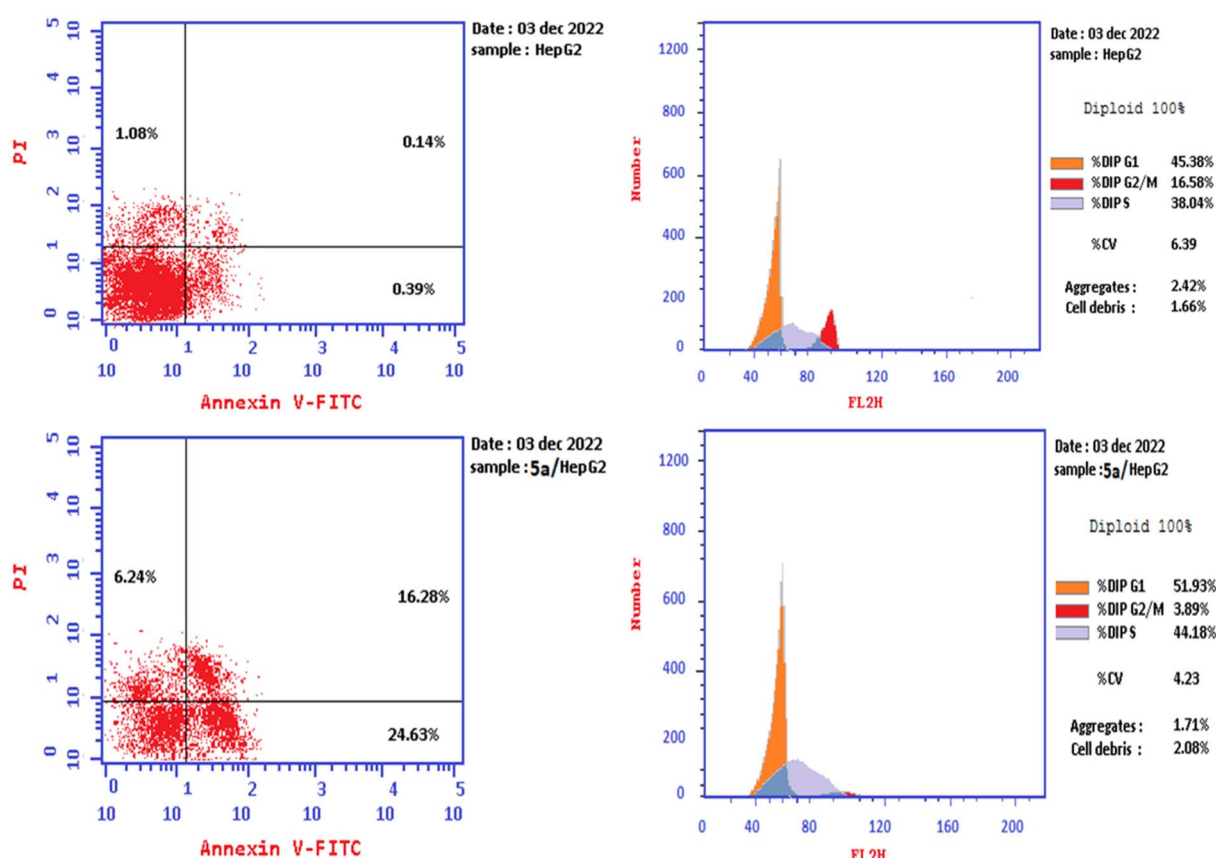
Fig. 4 The cell cycle analysis and apoptosis induction study of the control untreated and **5a**-treated HepG-2 cell line utilizing Annexin V/PI.

Table 3 The percentage of apoptosis and necrosis caused by compound **5a** in HepG-2 cancer cell line

	Apoptosis			
	Total	Early	Late	Necrosis
5a /HepG-2	47.15	24.63	16.28	6.24
Cont./HepG-2	1.61	0.39	0.14	1.08

HepG-2 cells were treated with the IC_{50} concentration of **5a** (3.42 μ M) for 24 h followed by staining with propidium iodide (PI). DNA contents were measured by flow cytometry (BECKMAN COULTER CytoFLEX).^{61,62} The impact of **5a** on the percentage of different cell growth phases (G0–G1, S, G2/M, and pre-G1) was recorded. The gained results were compared with non-treated HepG-2 cells. Fig. 3 is a representative cell cycle distribution histogram of the stained DNA content of the treated cancer cells with compound **5a**. The data obtained showed an observable increase in the percentage of cells from 45.38% in G0–G1 phase and 38.04% in S phase in the untreated HepG-2 cells to 51.93% and 44.18% in **5a**-treated HepG-2 cells, alongside a detectable decrease in DNA percentage from 16.58% in the untreated cells reaching 3.89% in the treated cells in G2/M phase. This result indicates cell cycle arrest at the G1/S phase. It is evident that the compound **5a** is an effective inhibitor of DNA synthesis or repair and induces programmed cell death and cell cycle arrest.

3.2.4. Apoptosis study of compound **5a.** To assure the ability of compound **5a** to induce apoptosis, the annexin-V/FTIC/PI dual staining assay was utilized. The use of annexin-V can help identify translocated phosphatidylserine (PS), a characteristic hallmark of apoptosis. The cells were labeled with FITC, annexin V, and PI. Apoptosis was validated in the cells that had lost membrane integrity by those that reacted positively for annexin V/PI.^{63,64}

The dot plot flow cytometry data of the stained cells is represented in Fig. 4. HepG-2 cancer cells were treated with the IC_{50} concentration of **5a** (3.42 μ M) and incubated for 24 h. The obtained data showed a significant increase in the percent of positive apoptotic cells in the early and late stages (lower and upper right quadrants of the cytogram) from 0.39 and 0.14% to 24.63 and 16.28%, respectively, which comprises about 63 and 116 folds with respect to the untreated cells (Fig. 4, Table 3). Moreover, there is an increase in the percentage of the necrotic cells from 1.08% (untreated cells) to 6.24% (**5a**-treated cells). This result exhibited that the total percentages of the early and late apoptotic cells are greater than the percentage of the necrotic cells, confirming that the apoptosis process is one of

the main mechanistic pathways of cell death caused by **5a** (Table 3).

3.2.5. The effect of compound **5a on the hallmarks of apoptosis induction: Bax, Bcl-2, p53, and caspase-3 levels.** The two major pathways that control the cell throughout the apoptosis process are the intrinsic pathway (by the mitochondria) and the extrinsic pathway (*via* the death receptor).

The mitochondrial apoptotic process is synchronised by the Bcl-2 protein family.

Two of these proteins, Bcl-2 and Bax, fine-tune this pre-determined process, with Bcl-2 acting as an anti-apoptotic and Bax as an inducer (pro-apoptotic). The ability of the cell to undergo apoptosis is determined by the precise balance between these two distinct proteins.^{65,66} The tumor suppressor gene, p53, is also an essential component of the cellular emergency response mechanism that results in cell death or the arrest of cell growth.

Cancer can be stopped in its tracks by p53 activation resulting in apoptosis, or a G1 cell cycle halt.

The retention of genomic integrity and p53 inactivation in malignancies may be the cause of accelerated cell proliferation and resistance to genotoxic anticancer therapies. An essential part of the cellular emergency response system that causes cell growth arrest or apoptosis is p53.⁶⁷

Furthermore, the Cysteinyl Aspartate-Specific Proteinase family, which includes Caspases-3, is essential for starting programmed cell death (apoptosis). All apoptotic processes, such as cell shrinkage, chromatin condensation, and DNA fragmentation, depend on caspase-3.^{68,69}

Accordingly, it was of interest to study the effects of compound **5a** on the hallmarks levels; Bax, Bcl-2, p53, and caspase-3 in HepG-2 cell line using ELISA process.^{67–69} HepG-2 cells were treated with the IC_{50} concentration of compound **5a** (3.42 μ M) for 24 h utilizing erlotinib as a reference drug. The obtained data were expressed in terms of pg mL^{-1} for Bax and p53 and as ng mL^{-1} for both Bcl-2 and caspase-3 levels in the **5a**-treated HepG-2 cells. It has been investigated that compound **5a** boosted the level of the pro-apoptotic protein Bax by ~5.4 folds and reduced the antiapoptotic protein Bcl-2 level by ~3.9 folds in the treated HepG-2 cells in comparison with the untreated cells. Due to its importance, the ratio of the two latter proteins Bax/Bcl-2 was calculated for compound **5a** to be 21 times higher than that in the untreated cells. This result confirmed that the compound **5a** has moved the cells toward apoptosis. Moreover, the results showed that compound **5a** upregulated the levels of p53 and caspase-3 in the tested HepG-2 cells by ~6.9 and 23.8 folds, respectively compared to the control (Table 4). The reported data in Table 4 represents that the activities of the

Table 4 The effect of the compound **5a** on the levels of some key hallmarks for apoptosis, Bax, Bcl-2, p53, and caspase-3

Compound 5a	Bax (pg mL^{-1})	Bcl-2 (ng mL^{-1})	Bax/Bcl-2	p53 (pg mL^{-1})	Casp-3 (ng mL^{-1})
5a /HepG-2	211.40 ± 0.25	2.09 ± 0.15	101.14	825.22 ± 0.40	42.60 ± 0.10
Cont./HepG-2	38.80 ± 0.10	8.16 ± 0.24	4.75	119.52 ± 0.02	1.79 ± 0.15
Erlotinib/HepG-2	200.20 ± 0.25	1.69 ± 0.10	118.84	890.30 ± 0.01	58.41 ± 0.12



evaluated compound **5a** was approximately similar to that obtained by the standard drug erlotinib (Table 4).

4. Computational studies

4.1. Molecular modeling studies

Utilizing the Molecular Operating Environment software (MOE-Dock) version 2014.0901,^{70,71} molecular docking was carried out to clarify the variance in the *in vitro* inhibitory activities of the evaluated compounds **5a** and **5b** against c-Met kinase. The native co-crystallized ligand, *N*-[3-fluoro-4-[(7-methoxyquinolin-4-yl)oxy]phenyl]-1-[(2*R*)-2-hydroxypropyl]-5-methyl-3-oxo-2-phenyl-2,3-dihydro-1*H*-pyrazole-4-carboxamide, was re-docked

in the active binding site of c-Met (PDB code: 3U6I)⁷² to validate the docking process. This resulted in energy score of -9.72 kcal mol $^{-1}$ at root mean square deviation (RMSD) value equal to 0.79 Å, indicating that the docking process was confirmed. Then, our targets **5a** and **5b** were docked and the results were depicted in Fig. 5 and 6.

As shown in Fig. 5 and 6, the screened promising targets **5a** and **5b** were fixed well within the active pocket of c-Met with favorable energy scores of -10.22 and -9.83 kcal mol $^{-1}$, respectively. It was observed in both derivatives that the sulfonyl-4-methylbenzene fragment at p-1 of the pyrazolo[3,4-*b*]pyridine core is located facing and surrounded by the essential amino acids **Lys1110**, **Leu1140**, **Leu1157**, **Met1211**, **Ala1221**, and

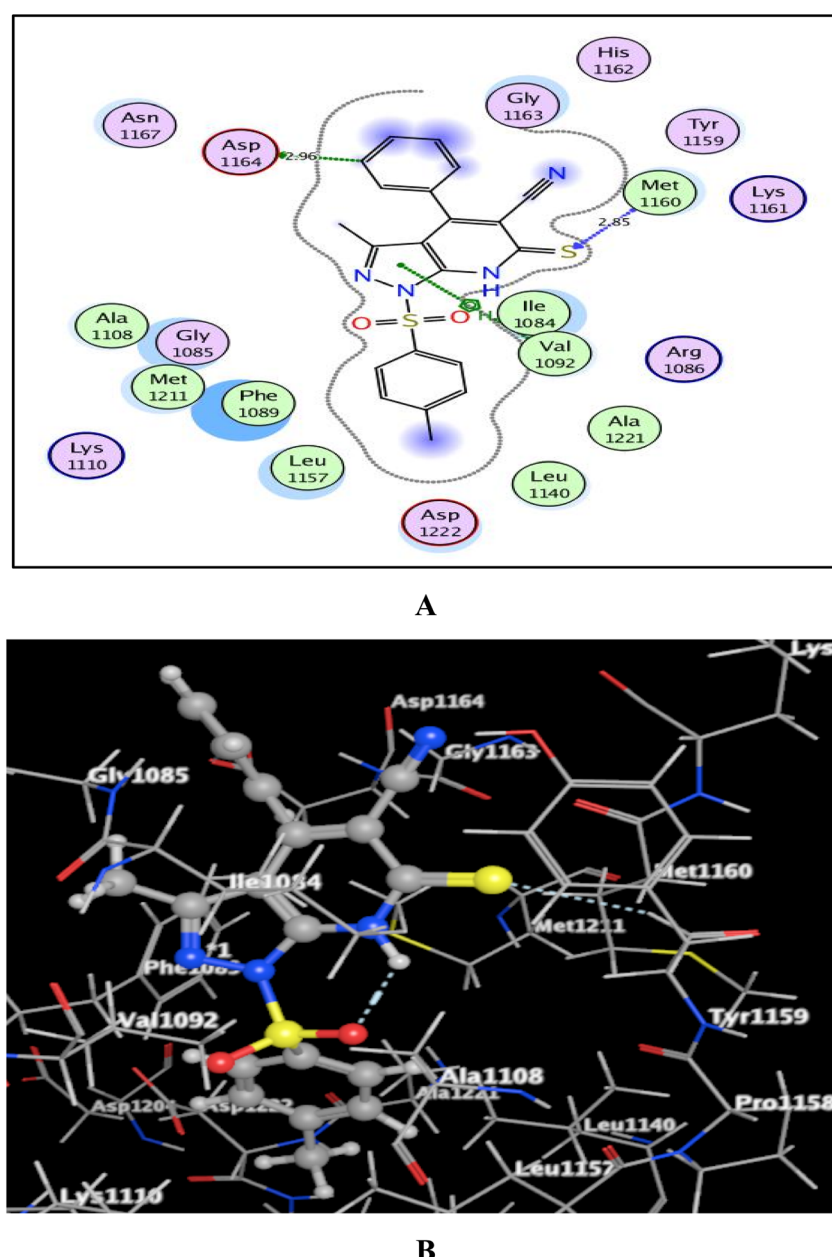
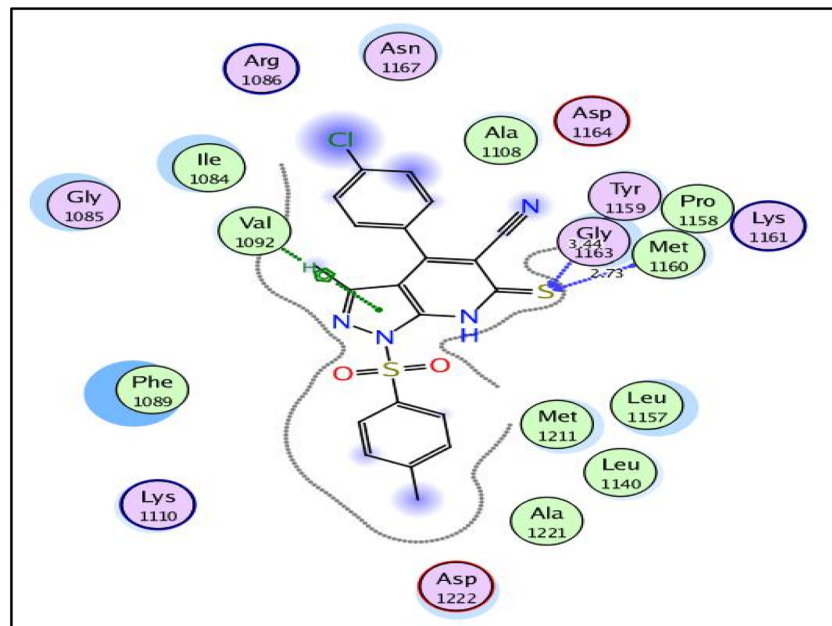
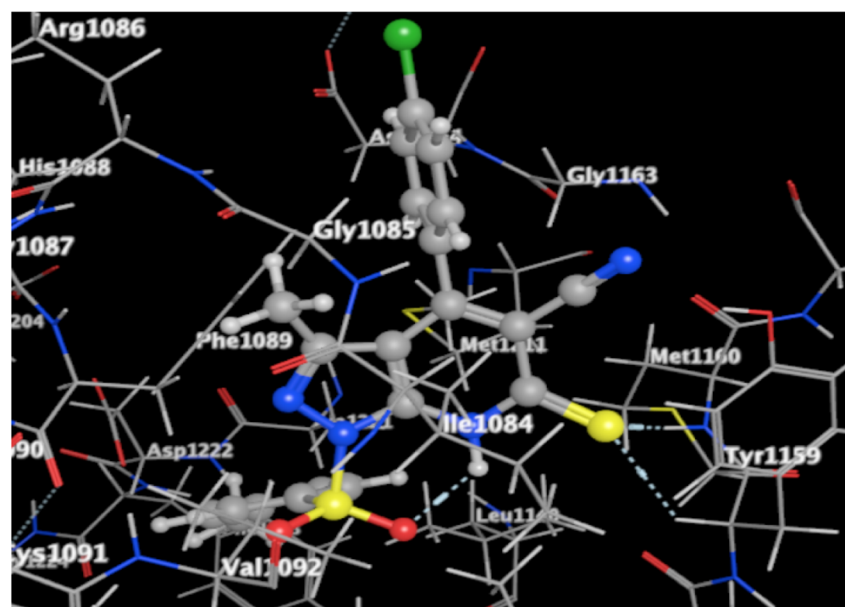


Fig. 5 (A) & (B) patterns illustrating the 2D and 3D binding interactions of the promising pyrazolo[3,4-*b*]pyridine target **5a** into active pocket of c-Met kinase (PDB code: 3U6I).





A



B

Fig. 6 (A) & (B) patterns illustrating the 2D and 3D binding interactions of the promising pyrazolo[3,4-*b*]pyridine target **5b** into active pocket of c-Met kinase (PDB code: 3U6I).

Asp1222 through hydrophobic interactions. On the other hand, the 6-thioxopyrazolo[3,4-*b*]pyridine-5-carbonitrile scaffold afforded arene-H interactions between the centroid of pyrazole and the amino acid **Val1092**. Moreover, the sulfur atom formed H-bond acceptor with the key amino acid **Met1160**. The phenyl ring at p-4 of pyrazolo[3,4-*b*]pyridine in **5a** illustrated an H-bond donor between C-3 and the sidechain of **Asp1164** (distance: 2.96 Å). While substitution of the phenyl ring with Cl atom in the *para* position devoted **5b** from the previous hydrogen binding, and that could be the reason for its lower inhibitory activity than **5a**.

4.2. *In silico* ADME prediction study

Studying absorption, distribution, metabolism, and excretion (ADME) for the targeted substances might provide important data regarding the ideal pharmaceutical choice. This predicted investigation was assisted through the utilization of SwissADME, a free online application.⁷³⁻⁷⁵ The Veber rule ($TPSA \leq 140 \text{ \AA}^2$ and number of rotatable bonds ≤ 10) and Lipinski's rule (molecule with number of hydrogen bond acceptors ≤ 10 , number of hydrogen bond donors ≤ 5 MW ≤ 500 and MLogP \leq

Table 5 Expected physicochemical properties and lipophilicity of pyrazolo[3,4-*b*]pyridine-5-carbonitrile derivatives **5a** and **5b**

Compd.	MW ^a	MLogP ^b	TPSA ^c (Å ²)	<i>n</i> _{HBD} ^d	<i>n</i> _{HBA} ^e	<i>n</i> _{RB} ^f	Violations ^g
5a	420.51	3.17	132.01	1	4	3	0
5b	518.54	1.66	137.57	0	8	6	1

^a Molecular weight. ^b Calculated lipophilicity (MLogP_{o/w}). ^c Topological polar surface area. ^d Number of hydrogen bond donor. ^e Number of hydrogen bond acceptor. ^f Number of rotatable bond. ^g Violations from Lipinski and Veber rules.

4.15) govern the optimal medication for oral administration. The 6-thioxopyrazolo[3,4-*b*]pyridine-5-carbonitrile target **5a** was found to be in compliance with the prior rules with no violations, while the derivative **5b** exhibited MW > 500 and one violation (Table 5).

Considering the bioavailability radar chart (Fig. 7), it was found that the pyrazolo[3,4-*b*]pyridine-5-carbonitrile derivatives **5a** and **5b** are located in the ideal range (pink zone) concerning to five key factors LIPO (lipophilicity), SIZE, POLAR (polarity),

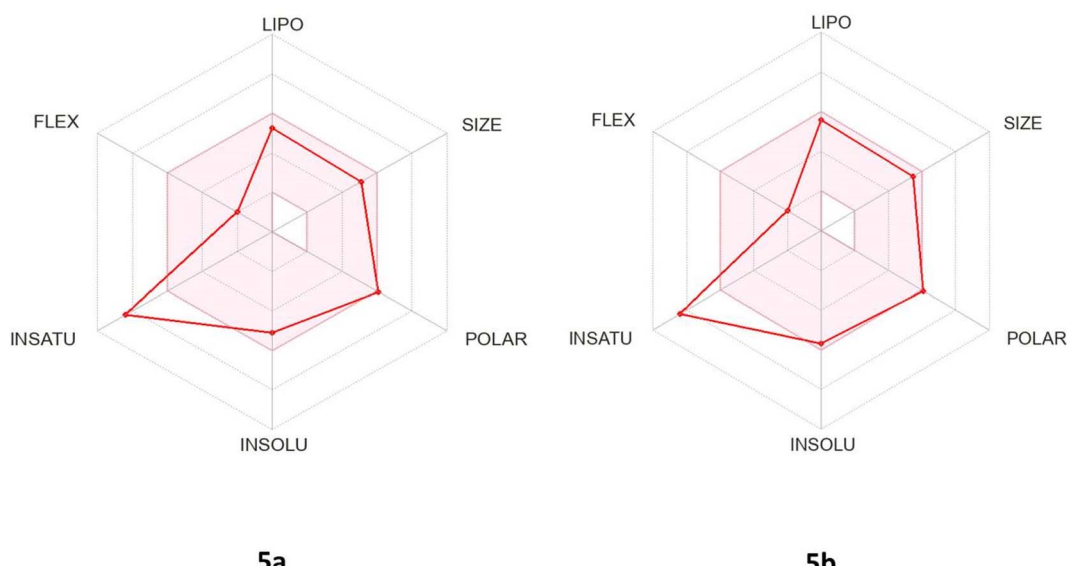


Fig. 7 The bioavailability radar chart of pyrazolo[3,4-*b*]pyridine-5-carbonitrile derivatives **5a** and **5b**. The pink region illustrated the optimal range for each of the oral bioavailability parameters and the predicted ones for the screened compounds were displayed as red lines.

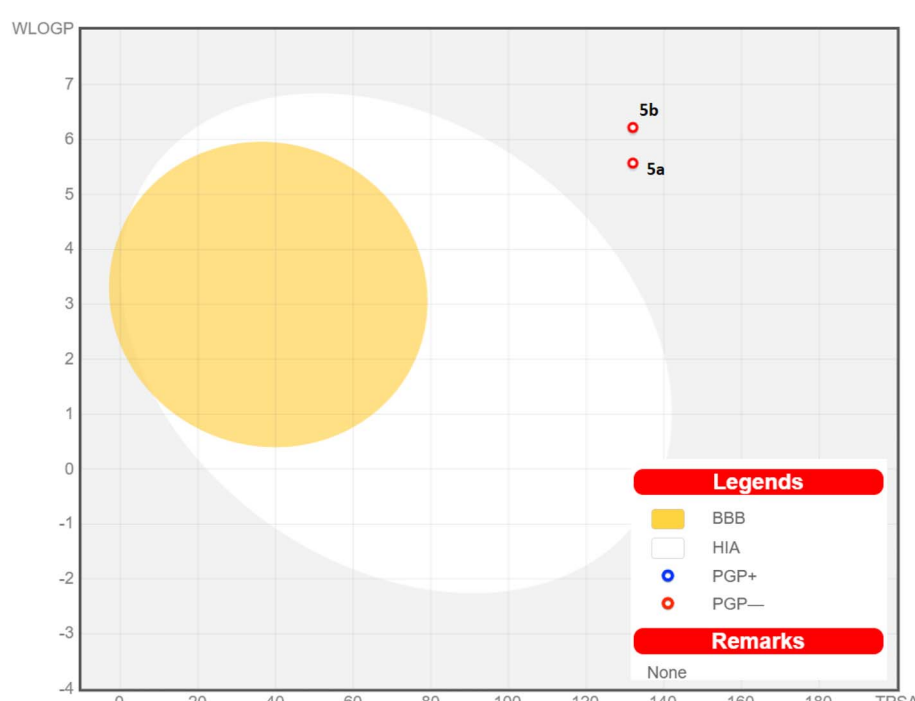


Fig. 8 Chart of boiled-egg revealing the BBB penetration capability and gastrointestinal absorption of pyrazolo[3,4-*b*]pyridine-5-carbonitrile derivatives **5a** and **5b**; PGP+: substrate of *p*-glycoprotein; PGP-: non-substrate of *p*-glycoprotein.



INSOLU (solubility) and FLEX (flexibility), but were distanced from the optimal region of INSATU (saturation).

The pharmacokinetic properties of the promising pyrazolo[3,4-*b*]pyridine-5-carbonitriles **5a** and **5b** were represented and analyzed in Fig. 8 and Table 6 (ESI†). All the screened compounds are predicted to be neither brain-penetrated nor gastrointestinally absorbed (outside the egg). Therefore, they are not predicted to be administered orally and could be used parenterally. Also, they are only employed to treat peripheral illnesses and are not thought to disrupt the central nervous system. These derivatives also got a satisfactory bioavailability grade of 0.55 and are not supposed to trigger a PAIN warning. Additionally, the red dots in Fig. 8 indicate that the two derivatives are not substrates for *p*-glycoprotein (*P*-gp, a drug efflux transporter), revealing a low chance of their efflux out of the cell with their highest activity.

5. Conclusion

In summary, a new set of derivatives bearing pyrazolo[3,4-*b*]pyridine, pyrazolo[3,4-*b*]thieno[3,2-*e*]pyridine, and pyrazolo[3,4-*d*]thiazole-5-thione scaffolds **5a,b**, **8a-f**, and **10a,b**, respectively, were designed, synthesized, and evaluated for their biological impacts as antiproliferative agents targeting c-Met inhibition. The screening of anticancer activity resulted in the identification of the two most promising compounds, **5a** and **5b**, with IC₅₀ values ranging from 3.42 ± 1.31 to 9.21 ± 0.02 μM against HepG-2, MCF-7, and HCT-116 human cancer cell lines. c-Met assay represented the promising inhibitory activities of both compounds, with IC₅₀ values of 4.27 ± 0.31 and 7.95 ± 0.17 nM, respectively. Meanwhile, cell cycle and apoptosis assays in HepG-2 cells by flow cytometry indicated that compound **5a** arrested the cell cycle at the G1/S phase, inducing apoptosis of the cells. In addition, **5a** up-regulated the levels of Bax/Bcl-2, p53, and caspase-3 in the tested HepG-2 cells by 21, 6.9, and 23.8 folds, respectively, compared to the untreated HepG-2 cells. Molecular docking study showed that both compounds **5a** and **5b** were fixed well within the active pocket of c-Met with favorable energy scores of -10.22 and -9.83 kcal mol⁻¹, respectively. In addition, the ADME prediction study showed that **5a** and **5b** fulfilled the criteria of the drug likeness approach. Accordingly, the pyrazolo[3,4-*b*]pyridine scaffold is a promising template in the field of drug discovery and optimization.

Conflicts of interest

The authors declare that they have no known competing financial interests or personal relationships that could have appeared to influence the work reported in this paper.

Acknowledgements

The research work was funded by institutional fund projects under grant no. IFPIP-1237-247-1443. Therefore, the authors gratefully acknowledge technical and financial support from the Ministry of Education and King Abdulaziz University, DSR, Jeddah, Saudi Arabia.

References

- Y. Dong, H. Hu, Y. Sun, M. Qin, P. Gong, Y. Hou and Y. Zhao, Design, synthesis and biological evaluation of novel c-Met/HDAC dual inhibitors, *Bioorg. Med. Chem. Lett.*, 2020, **30**(23), 127610.
- Z. Wang, J. Shi, X. Zhu, W. Zhao, Y. Gong, X. Hao, Y. Hou, Y. Liu, S. Ding, J. Liu and Y. Chen, Design, synthesis and biological evaluation of novel 4-phenoxypyridine based 3-oxo-3, 4-dihydroquinoxaline-2-carboxamide derivatives as potential c-Met kinase inhibitors, *Bioorg. Chem.*, 2020, **105**, 104371.
- M. Mortazavi, E. Raufi, T. Damghani, M. Khoshneviszadeh, N. Edraki, M. Eskandari, E. Giovannetti, G. J. Peters, S. Pirhadi and O. Firuzi, Discovery of anticancer agents with c-Met inhibitory potential by virtual and experimental screening of a chemical library, *Eur. J. Pharmacol.*, 2023, **938**, 175395.
- C. H. Gow, M. S. Hsieh, Y. L. Chen, Y. N. Liu, S. G. Wu and J. Y. Shih, Survival outcomes and prognostic factors of lung cancer patients with the MET exon 14 skipping mutation: A single-center real-world study, *Front. Oncol.*, 2023, **13**, 925.
- J. A. Bikker, N. Brooijmans, A. Wissner and T. S. Mansour, Kinase domain mutations in cancer: implications for small molecule drug design strategies, *J. Med. Chem.*, 2009, **52**, 1493–1509.
- R. Robert Jr, Properties of FDA-approved small molecule protein kinase inhibitors: A 2020 update, *Pharmacol. Res.*, 2020, **152**, 104609.
- P. Su, M. Zhang and X. Knag, Targeting c-Met in the treatment of urologic neoplasms: Current status and challenges, *Front. Oncol.*, 2023, **13**, 1071030.
- W. M. Rashed, C-MET as a potential target therapy toward personalized therapy in some pediatric tumors: An overview, *Crit. Rev. Oncol./Hematol.*, 2018, **131**, 7–15.
- S. Pilotto, L. Carbognin, N. Karachaliou, P. C. Ma, R. Rosell, G. Tortora and E. Bria, Tracking MET de-addiction in lung cancer: A road towards the oncogenic target, *Cancer Treat. Rev.*, 2017, **60**, 1–11.
- J. Hu, L. Chen, Z. Lu, H. Yao, Y. Hu, L. Feng, Y. Pang, J. Q. Wu, Z. Yu and W. H. Chen, Design, Synthesis and Antitumor Activity of Novel Selenium-Containing Tepotinib Derivatives as Dual Inhibitors of c-Met and TrxR, *Molecules*, 2023, **28**(3), 1304.
- H. Morgan and K. John, The conformational plasticity of protein kinases, *Cell*, 2002, **109**, 275–282.
- G. Manning, D. B. Whyte, R. Martinez, T. Hunter and S. Sudarsanam, The protein kinase complement of the human genome, *Science*, 2002, **298**, 1912–1934.
- S. Berthou, D. M. Aebersold, L. S. Schmidt, D. Stroka, C. Heigl, B. Streit, D. Stalder, G. Gruber, C. Liang, A. R. Howlett, D. Candas, R. H. Greiner, K. E. Lipson and Y. Zimmer, The Met kinase inhibitor SU11274 exhibits a selective inhibition pattern toward different receptor mutated variants, *Oncogene*, 2004, **23**, 5387–5393.



14 M. H. Norman, L. Liu, M. Lee, N. Xi, I. Fellows, N. D. D'Angelo, C. Dominguez, K. Rex, S. F. Bellon, T. S. Kim and I. Dussault, Structure-based design of novel class II c-Met inhibitors: 1. Identification of pyrazolone-based derivatives, *J. Med. Chem.*, 2012, **55**, 1858–1867.

15 N. Liu, Y. Wang, G. Huang, C. Ji, W. Fan, H. Li, Y. Cheng and H. Tian, Design, synthesis and biological evaluation of 1*H*-pyrrolo[2,3-*b*]pyridine and 1*H*-pyrazolo[3,4-*b*]pyridine derivatives as c-Met inhibitors, *Bioorg. Chem.*, 2016, **65**, 146–158.

16 F. M. Yakes, J. Chen, J. Tan, K. Yamaguchi, Y. Shi, P. Yu, F. Qian, F. Chu, F. Bentzien, B. Cancilla, J. Orf, A. You, A. D. Laird, S. Engst, L. Lee, J. Lesch, Y. C. Chou and A. H. Joly, Cabozantinib (XL184), a novel MET and VEGFR2 inhibitor, simultaneously suppresses metastasis, angiogenesis, and tumor growth, *Mol. Cancer Ther.*, 2011, **10**, 2298–2308.

17 F. Qian, S. Engst, K. Yamaguchi, P. Yu, K. A. Won, L. Mock, T. Lou, J. Tan, C. Li, D. Tam, J. Lougheed, F. M. Yakes, F. Bentzien, W. Xu, T. Zaks, R. Wooster, J. Greshock and A. H. Joly, Inhibition of tumor cell growth, invasion, and metastasis by EXEL-2880 (XL880, GSK1363089), a novel inhibitor of HGF and VEGF receptor tyrosine kinases, *Cancer Res.*, 2009, **69**, 8009–8016.

18 Z. Wang, J. Shi, X. Zhu, W. Zhao, Y. Gong, X. Hao, Y. Hou, Y. Liu, S. Ding, J. Liu and Y. Chen, Design, synthesis and biological evaluation of novel 4-phenoxypyridine based 3-oxo-3, 4-dihydroquinoxaline-2-carboxamide derivatives as potential c-Met kinase inhibitors, *Bioorg. Chem.*, 2020, **105**, 104371.

19 B. D. Smith, M. D. Kaufman, C. B. Leary, B. A. Turner, S. C. Wise, Y. M. Ahn, R. J. Booth, T. M. Caldwell, C. L. Ensinger, M. M. Hood, W. P. Lu, T. W. Patt, W. C. Patt, T. J. Rutkoski, T. Samarakoon, H. Telikepalli, L. Vogeti, S. Vogeti, K. M. Yates, L. Chun, L. J. Stewart, M. Clare and D. L. Flynn, Altiratinib inhibits tumor growth, invasion, angiogenesis, and microenvironment-mediated drug resistance *via* balanced inhibition of MET, TIE2, and VEGFR2, *Mol. Cancer Ther.*, 2015, **14**, 2023.

20 Y. Dai and D. W. Siemann, BMS-777607, a small-molecule met kinase inhibitor, suppresses hepatocyte growth factor-stimulated prostate cancer metastatic phenotype *in vitro*, *Mol. Cancer Ther.*, 2010, **9**, 1554–1561.

21 J. K. Rho, Y. J. Choi, S. Y. Kim, T. W. Kim, E. K. Choi, S. J. Yoon, B. M. Park, E. Park, J. H. Bae, C. M. Choi and J. C. Lee, MET and AXL inhibitor NPS-1034 exerts efficacy against lung cancer cells resistant to EGFR kinase inhibitors because of MET or AXL activation, *Cancer Res.*, 2014, **74**, 253–262.

22 Q. D. Tang, L. X. Wang, Y. L. Duan, W. H. Wang, S. M. Huang, J. Zhi, S. Jia, W. F. Zhu, P. Wang, R. Luo and P. W. Zheng, Discovery of novel 7-azaindole derivatives bearing dihydropyridazine moiety as c-Met kinase inhibitors, *Eur. J. Med. Chem.*, 2017, **133**, 97–106.

23 Q. D. Tang, L. X. Wang, Y. Y. Tu, W. F. Zhu, R. Luo, Q. D. Tu, P. Wang, C. J. Wu, P. Gong and P. W. Zheng, Discovery of novel pyrrolo[2,3-*b*]pyridine derivatives bearing 1,2,3-triazole moiety as c-Met kinase inhibitors, *Bioorg. Med. Chem. Lett.*, 2016, **26**, 1680–1684.

24 J. Liu, Y. L. Gong, J. T. Shi, X. C. Hao, Y. Wang, Y. P. Zhou, Y. L. Hou, Y. J. Liu, S. Ding and Y. Chen, Design, synthesis and biological evaluation of novel *N*-[4-(2-fluorophenoxy)pyridin-2-yl]cyclopropanecarboxamide derivatives as potential c-Met kinase inhibitors, *Eur. J. Med. Chem.*, 2020, **194**, 112244.

25 G. Luo, Y. Ma, X. Liang, G. Xie, Y. Luo, D. Zha, S. Wang, L. Yu, X. Zheng, W. Wu and C. Zhang, Design, synthesis and antitumor evaluation of novel 5-methylpyrazolo [1,5-*a*] pyrimidine derivatives as potential c-Met inhibitors, *Bioorg. Chem.*, 2020, **104**, 104356.

26 R. F. Barghash, W. M. Eldehna, M. Kovalova, V. Vojáčková, V. Kryštof and H. A. Abdel-Aziz, One-pot three-component synthesis of novel pyrazolo [3,4-*b*] pyridines as potent antileukemic agents, *Eur. J. Med. Chem.*, 2022, **227**, 113.

27 I. H. Eissa, A. M. El-Naggar and M. A. El-Hashash, Design, synthesis, molecular modeling and biological evaluation of novel 1*H*-pyrazolo[3,4-*b*]pyridine derivatives as potential anticancer agents, *Bioorg. Chem.*, 2016, **67**, 43–56.

28 A. Papastathopoulos, N. Lougiakis, I. K. Kostakis, P. Marakos, N. Pouli, H. Pratsinis and D. Kletsas, New bioactive 5-arylcarboximidamido pyrazolo[3,4-*c*]pyridines: synthesis, cytotoxic activity, mechanistic investigation and structure activity relationships, *Eur. J. Med. Chem.*, 2021, **218**, 113387.

29 M. Michailidou, V. Giannouli, V. Kotsikoris, O. Papadodima, G. Kontogianni, I. K. Kostakis, N. Lougiakis, A. Chatzioannou, F. N. Kolisis, P. Marakos, N. Pouli and H. Loutrari, Novel pyrazolopyridine derivatives as potential angiogenesis inhibitors: synthesis, biological evaluation and transcriptome-based mechanistic analysis, *Eur. J. Med. Chem.*, 2016, **121**, 143e15.

30 B. Zheng, Y. Peng, W. Wu, J. Ma, Y. Zhang, Y. Guo, S. Sun, Z. Chen, Q. Li and G. Hu, Synthesis and structure-activity relationships of pyrazolo[3,4-*b*]pyridine derivatives as adenosine 5'-monophosphate-activated protein kinase activators, *Arch. Pharm. Chem. Life Sci.*, 2019, **352**, 1900066.

31 Y. Li, H. Cheng, Z. Zhang, X. Zhuang, J. Luo, H. Long, Y. Zhou, Y. Xu, R. Taghipouran, D. Li, A. Patterson, J. Smaill, Z. Tu, D. Wu, X. Ren and K. Ding, N-(3-Ethynyl-2,4-difluorophenyl)sulfonamide derivatives as selective raf inhibitors, *ACS Med. Chem. Lett.*, 2015, **6**(5), 543–547.

32 H. Cheng, Y. Chang, L. Zhang, J. Luo, Z. Tu, X. Lu, Q. Zhang, J. Lu, X. Ren and K. Ding, Identification and optimization of new dual inhibitors of B-raf and epidermal growth factor receptor kinases for overcoming resistance against vemurafenib, *J. Med. Chem.*, 2014, **57**, 2692–2703.

33 A.-S. Huart, B. Saxty, A. Merritt, M. Nekulova, S. Lewis, Y. Huang, B. Vojtesek, C. Kettleborough and T. R. Hupp, A Casein kinase 1/Checkpoint kinase 1 pyrazolo-pyridine protein kinase inhibitor as novel activator of the p53 pathway, *Bioorg. Med. Chem. Lett.*, 2013, **23**, 5578–5585.

34 N. Liu, Y. Wang, G. Huang, C. Ji, W. Fan, H. Li, Y. Cheng and H. Tian, Design, synthesis and biological evaluation of 1*H*-pyrrolo[2,3-*b*]pyridine and 1*H*-pyrazolo[3,4-*b*]pyridine





derivatives as c-Met inhibitors, *Bioorg. Chem.*, 2016, **65**, 146–158.

35 B. Zhao, Y. Li, P. Xu, Y. Dai, C. Luo, Y. Sun, J. Ai, M. Geng and W. Duan, Discovery of substituted 1*H*-pyrazolo[3,4-*b*]pyridine derivatives as potent and selective FGFR kinase inhibitors, *ACS Med. Chem. Lett.*, 2016, **7**, 629–634.

36 M. S. Nafie, A. M. Amer, A. K. Mohamed and E. S. Tantawy, Discovery of novel pyrazolo[3,4-*b*]pyridine scaffold-based derivatives as potential PIM-1 kinase inhibitors in breast cancer MCF-7 cells, *Bioorg. Med. Chem.*, 2020, **28**, 115828.

37 J. Witherington, V. Bordas, D. Haigh, D. M. B. Hickey, R. J. Ife, A. D. Rawlings, B. P. Slingsby, D. G. Smith and R. W. Ward, 5-Aryl-pyrazolo[3,4-*b*]pyridazines: potent inhibitors of glycogen synthase kinase-3 (GSK-3), *Bioorg. Med. Chem. Lett.*, 2003, **13**, 1581–1584.

38 G. S. Hassan, H. H. Georgey, E. Z. Mohammed, R. F. George, W. R. Mahmoud and F. A. Omar, Mechanistic selectivity investigation and 2D-QSAR study of some new antiproliferative pyrazoles and pyrazolopyridines as potential CDK2 Inhibitors, *Eur. J. Med. Chem.*, 2021, **218**, 113389.

39 N. Liu, Y. Wang, G. Huang, C. Ji, W. Fan, H. Li, Y. Cheng and H. Tian, Design, synthesis and biological evaluation of 1*H*-pyrrolo[2,3-*b*]pyridine and 1*H*-pyrazolo[3,4-*b*]pyridine derivatives as c-Met inhibitors, *Bioorg. Chem.*, 2016, **65**, 146–158.

40 Y. Ma, G. Sun, D. Chen, X. Peng, Y. L. Chen, Y. Su, Y. Ji, J. Liang, X. Wang, L. Chen and J. Ding, Design and optimization of a series of 1-sulfonylpyrazolo[4,3-*b*]pyridines as selective c-Met inhibitors, *J. Med. Chem.*, 2015, **58**(5), 2513–2529.

41 R. M. Mohareb, K. M. Hilmy and Y. A. Elshehawy, Discovery of new thiophene, pyrazole, isoxazole derivatives as antitumor, c-Met, tyrosine kinase and Pim-1 kinase inhibitors, *Bull. Chem. Soc. Ethiop.*, 2018, **32**(2), 285–308.

42 J. Li, W. Lu, Y. Yang, R. Xiang, Y. Ling, C. Yu and Y. Zhou, Hybrid Nanomaterials for Cancer Immunotherapy, *Adv. Sci. Lett.*, 2022, **5**, 2204932.

43 H. Sung, J. Ferlay, R. L. Siegel, M. Laversanne, I. Soerjomataram, A. Jemal and F. Bray, *Ca-Cancer J. Clin.*, 2021, **71**, 209.

44 (a) W. Song, S. N. Musetti and L. Huang, Nanomaterials for cancer immunotherapy, *Biomaterials*, 2017, **148**, 16; (b) H. Phuengkham, L. Ren, I. W. Shin and Y. T. Lim, Nanoengineered immune niches for reprogramming the immunosuppressive tumor microenvironment and enhancing cancer immunotherapy, *Adv. Mater.*, 2019, **31**, 1803322.

45 S. Yan, X. Jiao, H. Zou and K. Li, Prognostic significance of c-Met in breast cancer: a meta-analysis of 6010 cases, *Diagn. Pathol.*, 2015, **10**, 62.

46 J. S. Pyo, G. Kang, W. J. Cho and S. B. Choi, Clinicopathological significance and concordance analysis of c-MET immunohistochemistry in non-small cell lung cancers: A meta-analysis, *Pathol. Res. Pract.*, 2016, **212**, 710–716.

47 S. Yu, Y. Yu, N. Zhao, J. Cui, W. Li and T. Liu, C-Met as a prognostic marker in gastric cancer: a systematic review and meta-analysis, *PLoS One*, 2013, **8**, e79137.

48 J. H. Kim, B. J. Kim and H. S. Kim, Clinicopathological impacts of high c-Met expression in head and neck squamous cell carcinoma: a meta-analysis and review, *Oncotarget*, 2017, **8**, 113120–113128.

49 J. Peng, S. Qi, P. Wang, W. Li, C. Liu and F. Li, Diagnosis and prognostic significance of c-Met in cervical cancer: a meta-analysis, *Dis. Markers*, 2016, **2016**, 6594016.

50 J. H. Kim, H. S. Kim, B. J. Kim, J. Lee and H. J. Jang, Prognostic value of c-Met overexpression in pancreatic adenocarcinoma: a meta-analysis, *Oncotarget*, 2017, **8**, 73098–73104.

51 J. H. Kim, H. S. Kim, B. J. Kim, H. J. Jang and J. Lee, Prognostic value of c-Met overexpression in hepatocellular carcinoma: a meta-analysis and review, *Oncotarget*, 2017, **8**, 351–357.

52 J. H. Kim, B. J. Kim and H. S. Kim, Clinicopathological impacts of high c-Met expression in renal cell carcinoma: a meta-analysis and review, *Oncotarget*, 2017, **8**, 75478–75487.

53 C. A. Larsen and R. H. Dashwood, Suppression of Met activation in human colon cancer cells treated with (–)-epigallocatechin-3-gallate: Minor role of hydrogen peroxide, *Biochem. Biophys. Res. Commun.*, 2009, **389**(3), 527–530.

54 A. A. El-Sayed, E. S. Nossier, A. A. Almehizia and A. E. G. E. Amr, Design, synthesis, anti-cancer evaluation and molecular docking study of novel 2,4-dichlorophenoxy-methyl-based derivatives linked to nitrogenous heterocyclic ring systems as potential CDK-2 inhibitors, *J. Mol. Struct.*, 2022, **1247**, 131285.

55 E. S. Nossier, S. M. El-hallouty and E. R. Zaki, Synthesis, anticancer evaluation and molecular modeling of some substituted thiazolidinonyl and thiazolyl pyrazole derivatives, *Int. J. Pharm. Pharm. Sci.*, 2015, **7**, 353–359.

56 I. M. Othman, Z. M. Alamshany, N. Y. Tashkandi, E. S. Nossier, M. M. Anwar and H. A. Radwan, Chemical synthesis and molecular docking study of new thiazole, thiophene, and thieno[2,3-*d*]pyrimidine derivatives as potential antiproliferative and antimicrobial agents, *J. Mol. Struct.*, 2022, **15**, 133926.

57 Y. Sun, Y. Liu, X. Ma and H. Hu, The influence of cell cycle regulation on chemotherapy, *Int. J. Mol. Sci.*, 2021, **22**(13), 6923.

58 I. M. Othman, Z. M. Alamshany, N. Y. Tashkandi, M. A. Gad-Elkareem, S. S. Abd El-Karim and E. S. Nossier, Synthesis and biological evaluation of new derivatives of thieno-thiazole and dihydrothiazolo-thiazole scaffolds integrated with a pyrazoline nucleus as anticancer and multi-targeting kinase inhibitors, *RSC Adv.*, 2022, **12**(1), 561–577.

59 E. A. Abd El-Meguid, G. O. Moustafa, H. M. Awad, E. R. Zaki and E. S. Nossier, Novel benzothiazole hybrids targeting EGFR: Design, synthesis, biological evaluation and molecular docking studies, *J. Mol. Struct.*, 2021, **1240**, 130595.

60 Z. M. Alamshany, N. Y. Tashkandi, I. M. Othman, M. M. Anwar and E. S. Nossier, New thiophene, thienopyridine and thiazoline-based derivatives: Design, synthesis and biological evaluation as antiproliferative agents and multitargeting kinase inhibitors, *Bioorg. Chem.*, 2022, **127**, 105964.

61 K. M. Amin, Y. M. Syam, M. M. Anwar, H. I. Ali, T. M. Abdel-Ghani and A. M. Serry, Synthesis and molecular docking study of new benzofuran and furo[3,2-g]chromone-based cytotoxic agents against breast cancer and p38 α MAP kinase inhibitors, *Bioorg. Chem.*, 2018, **76**, 487–500.

62 W. A. El-Sayed, F. M. Alminderej, M. M. Mounier, E. S. Nossier, S. M. Saleh and A. F. Kassem, Novel 1,2,3-triazole-coumarin hybrid glycosides and their tetrazolyl analogues: design, anticancer evaluation and molecular docking targeting EGFR, VEGFR-2 and CDK-2, *Molecules*, 2022, **27**(7), 2047.

63 W. A. El-Sayed, F. M. Alminderej, M. M. Mounier, E. S. Nossier, S. M. Saleh and A. F. Kassem, New 1,2,3-Triazole-Coumarin-Glycoside Hybrids and Their 1,2,4-triazolyl thioglycoside analogs targeting mitochondria apoptotic pathway: Synthesis, anticancer activity and docking simulation, *Molecules*, 2022, **27**(17), 5688.

64 Y. M. Syam, M. M. Anwar, S. S. Abd El-Karim, K. M. Elokely and S. H. Abdelwahed, New Quinoxaline-Based Derivatives as PARP-1 Inhibitors: Design, Synthesis, Antiproliferative, and Computational Studies, *Molecules*, 2022, **27**(15), 4924.

65 E. A. Abd El-Meguid, E. M. M. El-Deen, G. O. Moustafa, H. M. Awad and E. S. Nossier, Synthesis, anticancer evaluation and molecular docking of new benzothiazole scaffolds targeting FGFR-1, *Bioorg. Chem.*, 2022, **119**, 105504.

66 A. E. G. E. Amr, E. A. Elsayed, M. A. Al-Omar, H. O. Eldin Badr, E. S. Nossier and M. M. Abdallah, Design, synthesis, anticancer evaluation and molecular modeling of novel estrogen derivatives, *Molecules*, 2019, **24**(3), 416.

67 Z. He, W. Y. Ma, T. Hashimoto, A. M. Bode, C. S. Yang and Z. Dong, Induction of apoptosis by caffeine is mediated by the p53, Bax, and caspase 3 pathways, *Cancer Res.*, 2003, **63**(15), 4396–4401.

68 G. O. Moustafa, A. Shalaby, A. M. Naglah, M. M. Mounier, H. El-Sayed, M. M. Anwar and E. S. Nossier, Synthesis, characterization, *in vitro* anticancer potentiality, and antimicrobial activities of novel peptide-glycyrheticin-acid-based derivatives, *Molecules*, 2021, **26**(15), 4573.

69 A. S. Hassan, G. O. Moustafa, H. M. Awad, E. S. Nossier and M. F. Mady, Design, synthesis, anticancer evaluation, enzymatic assays, and a molecular modeling study of novel pyrazole-indole hybrids, *ACS Omega*, 2021, **6**, 12361–12374.

70 H. H. Elganzory, F. M. Alminderej, M. N. El-Bayaa, H. M. Awad, E. S. Nossier and W. A. El-Sayed, Design, synthesis, anticancer activity and molecular docking of new 1,2,3-triazole-based glycosides bearing 1,3,4-thiadiazolyl, indolyl and arylacetamide scaffolds, *Molecules*, 2022, **27**(20), 6960.

71 A. E. G. E. Amr, R. E. Abdel Mageid, M. El-Naggar, A. M. Naglah, E. S. Nossier and E. A. Elsayed, Chiral Pyridine-3,5-bis-(L-phenylalaninyl-L-leucinyl) Schiff Base Peptides as Potential Anticancer Agents: Design, synthesis, and molecular docking studies targeting lactate dehydrogenase-A, *Molecules*, 2020, **25**(5), 1096.

72 M. H. Norman, L. Liu, M. Lee, N. Xi, I. Fellows, N. D. D'Angelo, C. Dominguez, K. Rex, S. F. Bellon, T. S. Kim and I. Dussault, Structure-based design of novel class II c-Met inhibitors: 1. Identification of pyrazolone-based derivatives, *J. Med. Chem.*, 2012, **55**(5), 1858–1867.

73 A. Daina, O. Michielin and V. Zoete, SwissADME: a free web tool to evaluate pharmacokinetics, drug-likeness and medicinal chemistry friendliness of small molecules, *Sci. Rep.*, 2017, **7**(1), 1–13.

74 E. M. Mohi El-Deen, E. S. Nossier and E. A. Karam, New quinazolin-4(3H)-one derivatives incorporating hydrazone and pyrazole scaffolds as antimicrobial agents targeting DNA gyrase enzyme, *Sci. Pharm.*, 2022, **90**(3), 52.

75 I. M. Othman, M. A. Gad-Elkareem, A. E. G. E. Amr, M. A. Al-Omar, E. S. Nossier and E. A. Elsayed, Novel heterocyclic hybrids of pyrazole targeting dihydrofolate reductase: design, biological evaluation and *in silico* studies, *J. Enzyme Inhib. Med. Chem.*, 2020, **35**(1), 1491–1502.

